118. Hutchinson EC, Orr OE, Man Liu S, Engelhardt OG, Fodor E: **Characterization of the interaction between the influenza A virus polymerase subunit PB1 and the host nuclear import factor Ran-binding protein 5.** *J Gen Virol* 2011, **92**(Pt 8):1859–1869.
119. Ye Z, Robinson D, Wagner RR: **Nucleus-targeting domain of the matrix protein (M1) of influenza virus.** *J Virol* 1995, **69**(3):1964–1970.
120. Greenspan D, Krystal M, Nakada S, Arnheiter H, Lyles DS, Palese P: **Expression of influenza virus NS2 nonstructural protein in bacteria and localization of NS2 in infected eucaryotic cells.** *J Virol* 1985, **54**(3):833–843.
121. Greenspan D, Palese P, Krystal M: **Two nuclear location signals in the influenza virus NS1 nonstructural protein.** *J Virol* 1988, **62**(8):3020–3026.
122. Schneider J, Wolff T: **Nuclear functions of the influenza A and B viruses NS1 proteins: do they play a role in viral mRNA export?** *Vaccine* 2009, **27**(45):6312–6316.
123. Cao S, Liu X, Yu M, Li J, Jia X, Bi Y, Sun L, Gao GF, Liu W: **A nuclear export signal in the matrix protein of Influenza A virus is required for efficient virus replication.** *J Virol* 2012, **86**(9):4883–4891.
124. O'Neill RE, Talon J, Palese P: **The influenza virus NEP (NS2 protein) mediates the nuclear export of viral ribonucleoproteins.** *EMBO J* 1998, **17**(1):288–296.
125. Neumann G, Hughes MT, Kawaoka Y: **Influenza A virus NS2 protein mediates vRNP nuclear export through NES-independent interaction with hCRM1.** *EMBO J* 2000, **19**(24):6751–6758.
126. Iwatsuki-Horimoto K, Horimoto T, Fujii Y, Kawaoka Y: **Generation of influenza A virus NS2 (NEP) mutants with an altered nuclear export signal sequence.** *J Virol* 2004, **78**(18):10149–10155.
127. Chase GP, Rameix-Welti MA, Zvirbliene A, Zvirblis G, Gotz V, Wolff T, Naffakh N, Schwemmle M: **Influenza virus ribonucleoprotein complexes gain preferential access to cellular export machinery through chromatin targeting.** *PLoS Pathog* 2011, **7**(9):e1002187.
128. Bui M, Wills EG, Helenius A, Whittaker GR: **Role of the influenza virus M1 protein in nuclear export of viral ribonucleoproteins.** *J Virol* 2000, **74**(4):1781–1786.
129. Akarsu H, Burmeister WP, Petosa C, Petit I, Muller CW, Ruigrok RW, Baudin F: **Crystal structure of the M1 protein-binding domain of the influenza A virus nuclear export protein (NEP/NS2).** *EMBO J* 2003, **22**(18):4646–4655.
130. Baudin F, Petit I, Weissenhorn W, Ruigrok RW: **In vitro dissection of the membrane and RNP binding activities of influenza virus M1 protein.** *Virology* 2001, **281**(1):102–108.
131. Huang X, Liu T, Muller J, Levandowski RA, Ye Z: **Effect of influenza virus matrix protein and viral RNA on ribonucleoprotein formation and nuclear export.** *Virology* 2001, **287**(2):405–416.
132. Wu CY, Jeng KS, Lai MM: **The SUMOylation of matrix protein M1 modulates the assembly and morphogenesis of influenza A virus.** *J Virol* 2011, **85**(13):6618–6628.
133. Paterson D, Fodor E: **Emerging roles for the influenza A virus nuclear export protein (NEP).** *PLoS Pathog* 2012, **8**(12):e1003019.
134. Bui M, Myers JE, Whittaker GR: **Nucleo-cytoplasmic localization of influenza virus nucleoprotein depends on cell density and phosphorylation.** *Virus Res* 2002, **84**(1–2):37–44.
135. Pleschka S, Wolff T, Ehrhardt C, Hobom G, Planz O, Rapp UR, Ludwig S: **Influenza virus propagation is impaired by inhibition of the Raf/MEK/ERK signalling cascade.** *Nat Cell Biol* 2001, **3**(3):301–305.
136. Reinhardt J, Wolff T: **The influenza A virus M1 protein interacts with the cellular receptor of activated C kinase (RACK) 1 and can be phosphorylated by protein kinase C.** *Vet Microbiol* 2000, **74**(1–2):87–100.
137. Whittaker G, Kemler I, Helenius A: **Hyperphosphorylation of mutant influenza virus matrix protein, M1, causes its retention in the nucleus.** *J Virol* 1995, **69**(1):439–445.
138. Kawaguchi A, Matsumoto K, Nagata K: **YB-1 functions as a porter to lead influenza virus ribonucleoprotein complexes to microtubules.** *J Virol* 2012, **86**(20):11086–11095.
139. Klenk HD, Wagner R, Heuer D, Wolff T: **Importance of hemagglutinin glycosylation for the biological functions of influenza virus.** *Virus Res* 2002, **82**(1–2):73–75.
140. Wagner R, Matrosovich M, Klenk HD: **Functional balance between haemagglutinin and neuraminidase in influenza virus infections.** *Rev Med Virol* 2002, **12**(3):159–166.
141. Stieneke-Grober A, Vey M, Angliker H, Shaw E, Thomas G, Roberts C, Klenk HD, Garten W: **Influenza virus hemagglutinin with multibasic cleavage site is activated by furin, a subtilisin-like endoprotease.** *EMBO J* 1992, **11**(7):2407–2414.
142. Webster RG, Rott R: **Influenza virus A pathogenicity: the pivotal role of hemagglutinin.** *Cell* 1987, **50**(5):665–666.
143. Horimoto T, Kawaoka Y: **Reverse genetics provides direct evidence for a correlation of hemagglutinin cleavability and virulence of an avian influenza A virus.** *J Virol* 1994, **68**(5):3120–3128.
144. Momose F, Kikuchi Y, Komase K, Morikawa Y: **Visualization of microtubule-mediated transport of influenza viral progeny ribonucleoprotein.** *Microbes Infect* 2007, **9**(12–13):1422–1433.
145. Amorim MJ, Bruce EA, Read EK, Foeglein A, Mahen R, Stuart AD, Digard P: **A Rab11- and microtubule-dependent mechanism for cytoplasmic transport of influenza A virus viral RNA.** *J Virol* 2011, **85**(9):4143–4156.
146. van Zeijl MJ, Matlin KS: **Microtubule perturbation inhibits intracellular transport of an apical membrane glycoprotein in a substrate-dependent manner in polarized Madin-Darby canine kidney epithelial cells.** *Cell Regul* 1990, **1**(12):921–936.
147. Sun E, He J, Zhuang X: **Dissecting the role of COPI complexes in influenza virus infection.** *J Virol* 2013, **87**(5):2673–2685.
148. Eisfeld AJ, Kawakami E, Watanabe T, Neumann G, Kawaoka Y: **RAB11A is essential for transport of the influenza virus genome to the plasma membrane.** *J Virol* 2011, **85**(13):6117–6126.
149. Momose F, Sekimoto T, Ohkura T, Jo S, Kawaguchi A, Nagata K, Morikawa Y: **Apical transport of influenza A virus ribonucleoprotein requires Rab11-positive recycling endosome.** *PLoS One* 2011, **6**(6):e21123.
150. Bruce EA, Digard P, Stuart AD: **The Rab11 pathway is required for influenza A virus budding and filament formation.** *J Virol* 2010, **84**(12):5848–5859.
151. Eisfeld AJ, Neumann G, Kawaoka Y: **Human immunodeficiency virus rev-binding protein is essential for influenza a virus replication and promotes genome trafficking in late-stage infection.** *J Virol* 2011, **85**(18):9588–9598.
152. Leser GP, Lamb RA: **Influenza virus assembly and budding in raft-derived microdomains: a quantitative analysis of the surface distribution of HA, NA and M2 proteins.** *Virology* 2005, **342**(2):215–227.
153. Barman S, Ali A, Hui EK, Adhikary L, Nayak DP: **Transport of viral proteins to the apical membranes and interaction of matrix protein with glycoproteins in the assembly of influenza viruses.** *Virus Res* 2001, **77**(1):61–69.
154. Barman S, Nayak DP: **Analysis of the transmembrane domain of influenza virus neuraminidase, a type II transmembrane glycoprotein, for apical sorting and raft association.** *J Virol* 2000, **74**(14):6538–6545.
155. Lin S, Naim HY, Rodriguez AC, Roth MG: **Mutations in the middle of the transmembrane domain reverse the polarity of transport of the influenza virus hemagglutinin in MDCK epithelial cells.** *J Cell Biol* 1998, **142**(1):51–57.
156. Takeda M, Leser GP, Russell CJ, Lamb RA: **Influenza virus hemagglutinin concentrates in lipid raft microdomains for efficient viral fusion.** *Proc Natl Acad Sci USA* 2003, **100**(25):14610–14617.
157. Zhang J, Pekosz A, Lamb RA: **Influenza virus assembly and lipid raft microdomains: a role for the cytoplasmic tails of the spike glycoproteins.** *J Virol* 2000, **74**(10):4634–4644.
158. Barman S, Adhikary L, Chakrabarti AK, Bernas C, Kawaoka Y, Nayak DP: **Role of transmembrane domain and cytoplasmic tail amino acid sequences of influenza a virus neuraminidase in raft association and virus budding.** *J Virol* 2004, **78**(10):5258–5269.
159. Kundu A, Avalos RT, Sanderson CM, Nayak DP: **Transmembrane domain of influenza virus neuraminidase, a type II protein, possesses an apical sorting signal in polarized MDCK cells.** *J Virol* 1996, **70**(9):6508–6515.
160. Scheiffele P, Roth MG, Simons K: **Interaction of influenza virus haemagglutinin with sphingolipid-cholesterol membrane domains via its transmembrane domain.** *EMBO J* 1997, **16**(18):5501–5508.
161. Fujii Y, Goto H, Watanabe T, Yoshida T, Kawaoka Y: **Selective incorporation of influenza virus RNA segments into virions.** *Proc Natl Acad Sci USA* 2003, **100**(4):2002–2007.
162. Hutchinson EC, von Kirchbach JC, Gog JR, Digard P: **Genome packaging in influenza A virus.** *J Gen Virol* 2010, **91**(Pt 2):313–328.
163. Enami M, Enami K: **Influenza virus hemagglutinin and neuraminidase glycoproteins stimulate the membrane association of the matrix protein.** *J Virol* 1996, **70**(10):6653–6657.
164. Ruigrok RW, Barge A, Durrer P, Brunner J, Ma K, Whittaker GR: **Membrane interaction of influenza virus M1 protein.** *Virology* 2000, **267**(2):289–298.
165. Zhang J, Lamb RA: **Characterization of the membrane association of the influenza virus matrix protein in living cells.** *Virology* 1996, **225**(2):255–266.

166. Ye Z, Liu T, Offringa DP, McInnis J, Levandowski RA: **Association of influenza virus matrix protein with ribonucleoproteins.** *J Virol* 1999, **73**(9):7467–7473.
167. Cros JF, Palese P: **Trafficking of viral genomic RNA into and out of the nucleus: influenza, Thogoto and Borna disease viruses.** *Virus Res* 2003, **95**(1–2):3–12.
168. Nayak DP, Hui EK, Barman S: **Assembly and budding of influenza virus.** *Virus Res* 2004, **106**(2):147–165.
169. Yasuda J, Nakada S, Kato A, Toyoda T, Ishihama A: **Molecular assembly of influenza virus: association of the NS2 protein with virion matrix.** *Virology* 1993, **196**(1):249–255.
170. McCown MF, Pekosz A: **The influenza A virus M2 cytoplasmic tail is required for infectious virus production and efficient genome packaging.** *J Virol* 2005, **79**(6):3595–3605.
171. Schroeder C, Heider H, Moncke-Buchner E, Lin TI: **The influenza virus ion channel and maturation cofactor M2 is a cholesterol-binding protein.** *Eur Biophys J* 2005, **34**(1):52–66.
172. Rossman JS, Jing X, Leser GP, Lamb RA: **Influenza virus M2 protein mediates ESCRT-independent membrane scission.** *Cell* 2010, **142**(6):902–913.
173. Saito T, Kawano K: **Loss of glycosylation at Asn144 alters the substrate preference of the N8 influenza A virus neuraminidase.** *J Vet Med Sci* 1997, **59**(10):923–926.
174. Veit M: **Palmitoylation of virus proteins.** *Biol Cell* 2012, **104**(9):493–515.
175. Pal S, Santos A, Rosas JM, Ortiz-Guzman J, Rosas-Acosta G: **Influenza A virus interacts extensively with the cellular SUMOylation system during infection.** *Virus Res* 2011, **158**(1–2):12–27.
176. Xu K, Klenk C, Liu B, Keiner B, Cheng J, Zheng BJ, Li L, Han Q, Wang C, Li T, *et al*: **Modification of nonstructural protein 1 of influenza A virus by SUMO1.** *J Virol* 2011, **85**(2):1086–1098.
177. Pal S, Rosas JM, Rosas-Acosta G: **Identification of the non-structural influenza A viral protein NS1A as a bona fide target of the Small Ubiquitin-like MOdifier by the use of dicistronic expression constructs.** *J Virol Methods* 2010, **163**(2):498–504.
178. Gregoriades A, Guzman GG, Paoletti E: **The phosphorylation of the integral membrane (M1) protein of influenza virus.** *Virus Res* 1990, **16**(1):27–41.
179. Sugiyama K, Kamada T, Shimizu K, Watanabe Y: **Preferential phosphorylation of NP-protein of influenza A2 virus by virion-associated protein kinase.** *Jpn J Microbiol* 1976, **20**(3):227–232.
180. Privalsky ML, Penhoet EE: **The structure and synthesis of influenza virus phosphoproteins.** *J Biol Chem* 1981, **256**(11):5368–5376.
181. Almond JW, Felsenreich V: **Phosphorylation of the nucleoprotein of an avian influenza virus.** *J Gen Virol* 1982, **60**(Pt 2):295–305.
182. Kistner O, Muller K, Scholtissek C: **Differential phosphorylation of the nucleoprotein of influenza A viruses.** *J Gen Virol* 1989, **70**(Pt 9):2421–2431.
183. Arrese M, Portela A: **Serine 3 is critical for phosphorylation at the N-terminal end of the nucleoprotein of influenza virus A/Victoria/3/75.** *J Virol* 1996, **70**(6):3385–3391.
184. Hsiang TY, Zhou L, Krug RM: **Roles of the phosphorylation of specific serines and threonines in the NS1 protein of human influenza A viruses.** *J Virol* 2012, **86**(19):10370–10376.
185. Mitzner D, Dudek SE, Studtrucker N, Anhlan D, Mazur I, Wissing J, Jansch L, Wixler L, Bruns K, Sharma A, *et al*: **Phosphorylation of the influenza A virus protein PB1-F2 by PKC is crucial for apoptosis promoting functions in monocytes.** *Cell Microbiol* 2009, **11**(10):1502–1516.
186. Mahmoudian S, Auerochs S, Grone M, Marschall M: **Influenza A virus proteins PB1 and NS1 are subject to functionally important phosphorylation by protein kinase C.** *J Gen Virol* 2009, **90**(Pt 6):1392–1397.
187. Hale BG, Knebel A, Botting CH, Galloway CS, Precious BL, Jackson D, Elliott RM, Randall RE: **CDK/ERK-mediated phosphorylation of the human influenza A virus NS1 protein at threonine-215.** *Virology* 2009, **383**(1):6–11.
188. Garcia-Sastre A: **Induction and evasion of type I interferon responses by influenza viruses.** *Virus Res* 2011, **162**(1–2):12–18.
189. Ehrhardt C, Seyer R, Hrincius ER, Eierhoff T, Wolff T, Ludwig S: **Interplay between influenza A virus and the innate immune signaling.** *Microbes Infect* 2010, **12**(1):81–87.
190. Yan N, Chen ZJ: **Intrinsic antiviral immunity.** *Nature Immunol* 2012, **13**(3):214–222.
191. Guillot L, Le Goffic R, Bloch S, Escriou N, Akira S, Chignard M, Si-Tahar M: **Involvement of toll-like receptor 3 in the immune response of lung epithelial cells to double-stranded RNA and influenza A virus.** *J Biol Chem* 2005, **280**(7):5571–5580.
192. Le Goffic R, Balloy V, Lagranderie M, Alexopoulou L, Escriou N, Flavell R, Chignard M, Si-Tahar M: **Detrimental contribution of the Toll-like receptor (TLR)3 to influenza A virus-induced acute pneumonia.** *PLoS Pathog* 2006, **2**(6):e53.
193. Diebold SS, Kaisho T, Hemmi H, Akira S, Reis e Sousa C: **Innate antiviral responses by means of TLR7-mediated recognition of single-stranded RNA.** *Science* 2004, **303**(5663):1529–1531.
194. Lund JM, Alexopoulou L, Sato A, Karow M, Adams NC, Gale NW, Iwasaki A, Flavell RA: **Recognition of single-stranded RNA viruses by Toll-like receptor 7.** *Proc Natl Acad Sci USA* 2004, **101**(15):5598–5603.
195. Pichlmair A, Schulz O, Tan CP, Naslund TI, Liljestrom P, Weber F, Reis e Sousa C: **RIG-I-mediated antiviral responses to single-stranded RNA bearing 5'-phosphates.** *Science* 2006, **314**(5801):997–1001.
196. Kato H, Takeuchi O, Sato S, Yoneyama M, Yamamoto M, Matsui K, Uematsu S, Jung A, Kawai T, Ishii KJ, *et al*: **Differential roles of MDA5 and RIG-I helicases in the recognition of RNA viruses.** *Nature* 2006, **441**(7089):101–105.
197. Opitz B, Rejaibi A, Dauber B, Eckhard J, Vinzing M, Schmeck B, Hippenstiel S, Suttorp N, Wolff T: **IFNbeta induction by influenza A virus is mediated by RIG-I which is regulated by the viral NS1 protein.** *Cell Microbiol* 2007, **9**(4):930–938.
198. Le Goffic R, Pothlichet J, Vitour D, Fujita T, Meurs E, Chignard M, Si-Tahar M: **Cutting Edge: Influenza A virus activates TLR3-dependent inflammatory and RIG-I-dependent antiviral responses in human lung epithelial cells.** *J Immunol* 2007, **178**(6):3368–3372.
199. Pirhonen J, Sareneva T, Kurimoto M, Julkunen I, Matikainen S: **Virus infection activates IL-1 beta and IL-18 production in human macrophages by a caspase-1-dependent pathway.** *J Immunol* 1999, **162**(12):7322–7329.
200. Ichinohe T, Lee HK, Ogura Y, Flavell R, Iwasaki A: **Inflammasome recognition of influenza virus is essential for adaptive immune responses.** *J Exp Med* 2009, **206**(1):79–87.
201. Allen IC, Scull MA, Moore CB, Holl EK, McElvania-TeKippe E, Taxman DJ, Guthrie EH, Pickles RJ, Ting JP: **The NLRP3 inflammasome mediates in vivo innate immunity to influenza A virus through recognition of viral RNA.** *Immunity* 2009, **30**(4):556–565.
202. Thomas PG, Dash P, Aldridge JR Jr, Ellebedy AH, Reynolds C, Funk AJ, Martin WJ, Lamkanfi M, Webby RJ, Boyd KL, *et al*: **The intracellular sensor NLRP3 mediates key innate and healing responses to influenza A virus via the regulation of caspase-1.** *Immunity* 2009, **30**(4):566–575.
203. Ichinohe T, Pang IK, Iwasaki A: **Influenza virus activates inflammasomes via its intracellular M2 ion channel.** *Nature Immunol* 2010, **11**(5):404–410.
204. García-Sastre A: **Inhibition of interferon-mediated antiviral responses by influenza A viruses and other negative-strand RNA viruses.** *Virology* 2001, **279**(2):375–384.
205. Hale BG, Randall RE, Ortin J, Jackson D: **The multifunctional NS1 protein of influenza A viruses.** *J Gen Virol* 2008, **89**(Pt 10):2359–2376.
206. Mibayashi M, Martinez-Sobrido L, Loo YM, Cardenas WB, Gale M Jr, Garcia-Sastre A: **Inhibition of retinoic acid-inducible gene I-mediated induction of beta interferon by the NS1 protein of influenza A virus.** *J Virol* 2007, **81**(2):514–524.
207. Gack MU, Albrecht RA, Urano T, Inn KS, Huang IC, Carnero E, Farzan M, Inoue S, Jung JU, Garcia-Sastre A: **Influenza A virus NS1 targets the ubiquitin ligase TRIM25 to evade recognition by the host viral RNA sensor RIG-I.** *Cell Host Microbe* 2009, **5**(5):439–449.
208. Stasakova J, Ferko B, Kittel C, Sereinig S, Romanova J, Katinger H, Egorov A: **Influenza A mutant viruses with altered NS1 protein function provoke caspase-1 activation in primary human macrophages, resulting in fast apoptosis and release of high levels of interleukins 1beta and 18.** *J Gen Virol* 2005, **86**(Pt 1):185–195.
209. Lu Y, Wambach M, Katze MG, Krug RM: **Binding of the influenza virus NS1 protein to double-stranded RNA inhibits the activation of the protein kinase that phosphorylates the eIF-2 translation initiation factor.** *Virology* 1995, **214**(1):222–228.
210. Hatada E, Saito S, Fukuda R: **Mutant influenza viruses with a defective NS1 protein cannot block the activation of PKR in infected cells.** *J Virol* 1999, **73**(3):2425–2433.
211. Bergmann M, Garcia-Sastre A, Carnero E, Pehamberger H, Wolff K, Palese P, Muster T: **Influenza virus NS1 protein counteracts PKR-mediated inhibition of replication.** *J Virol* 2000, **74**(13):6203–6206.

212. Li S, Min JY, Krug RM, Sen GC: **Binding of the influenza A virus NS1 protein to PKR mediates the inhibition of its activation by either PACT or double-stranded RNA.** *Virology* 2006, **349**(1):13–21.
213. Tan SL, Katze MG: **Biochemical and genetic evidence for complex formation between the influenza A virus NS1 protein and the interferon-induced PKR protein kinase.** *J Interferon Cytokine Res* 1998, **18**(9):757–766.
214. Min JY, Li S, Sen GC, Krug RM: **A site on the influenza A virus NS1 protein mediates both inhibition of PKR activation and temporal regulation of viral RNA synthesis.** *Virology* 2007, **363**(1):236–243.
215. Min JY, Krug RM: **The primary function of RNA binding by the influenza A virus NS1 protein in infected cells: Inhibiting the 2'-5' oligo (A) synthetase/RNase L pathway.** *Proc Natl Acad Sci USA* 2006, **103**(18):7100–7105.
216. Zhao C, Hsiang TY, Kuo RL, Krug RM: **ISG15 conjugation system targets the viral NS1 protein in influenza A virus-infected cells.** *Proc Natl Acad Sci USA* 2010, **107**(5):2253–2258.
217. Tang Y, Zhong G, Zhu L, Liu X, Shan Y, Feng H, Bu Z, Chen H, Wang C: **Herc5 attenuates influenza A virus by catalyzing ISGylation of viral NS1 protein.** *J Immunol* 2010, **184**(10):5777–5790.
218. Hale BG, Jackson D, Chen YH, Lamb RA, Randall RE: **Influenza A virus NS1 protein binds p85beta and activates phosphatidylinositol-3-kinase signaling.** *Proc Natl Acad Sci USA* 2006, **103**(38):14194–14199.
219. Ehrhardt C, Marjuki H, Wolff T, Nurnberg B, Planz O, Pleschka S, Ludwig S: **Bivalent role of the phosphatidylinositol-3-kinase (PI3K) during influenza virus infection and host cell defence.** *Cell Microbiol* 2006, **8**(8):1336–1348.
220. Shin YK, Liu Q, Tikoo SK, Babiuk LA, Zhou Y: **Effect of the phosphatidylinositol 3-kinase/Akt pathway on influenza A virus propagation.** *J Gen Virol* 2007, **88**(Pt 3):942–950.
221. Shin YK, Liu Q, Tikoo SK, Babiuk LA, Zhou Y: **Influenza A virus NS1 protein activates the phosphatidylinositol 3-kinase (PI3K)/Akt pathway by direct interaction with the p85 subunit of PI3K.** *J Gen Virol* 2007, **88**(Pt 1):13–18.
222. Ehrhardt C, Wolff T, Ludwig S: **Activation of phosphatidylinositol 3-kinase signaling by the nonstructural NS1 protein is not conserved among type A and B influenza viruses.** *J Virol* 2007, **81**(21):12097–12100.
223. Ehrhardt C, Wolff T, Pleschka S, Planz O, Beermann W, Bode JG, Schmolke M, Ludwig S: **Influenza A virus NS1 protein activates the PI3K/Akt pathway to mediate antiapoptotic signaling responses.** *J Virol* 2007, **81**(7):3058–3067.
224. Hale BG, Batty IH, Downes CP, Randall RE: **Binding of influenza A virus NS1 protein to the inter-SH2 domain of p85 suggests a novel mechanism for phosphoinositide 3-kinase activation.** *J Biol Chem* 2008, **283**(3):1372–1380.
225. Hale BG, Randall RE: **PI3K signalling during influenza A virus infections.** *Biochem Soc Trans* 2007, **35**(Pt 2):186–187.
226. Li Y, Anderson DH, Liu Q, Zhou Y: **Mechanism of influenza A virus NS1 protein interaction with the p85beta, but not the p85alpha, subunit of phosphatidylinositol 3-kinase (PI3K) and up-regulation of PI3K activity.** *J Biol Chem* 2008, **283**(34):23397–23409.
227. Shin YK, Li Y, Liu Q, Anderson DH, Babiuk LA, Zhou Y: **SH3 binding motif 1 in influenza A virus NS1 protein is essential for PI3K/Akt signaling pathway activation.** *J Virol* 2007, **81**(23):12730–12739.
228. Hale BG, Kerry PS, Jackson D, Precious BL, Gray A, Killip MJ, Randall RE, Russell RJ: **Structural insights into phosphoinositide 3-kinase activation by the influenza A virus NS1 protein.** *Proc Natl Acad Sci USA* 2010, **107**(5):1954–1959.
229. Hrincius ER, Dierkes R, Anhlan D, Wixler V, Ludwig S, Ehrhardt C: **Phosphatidylinositol-3-kinase (PI3K) is activated by influenza virus vRNA via the pathogen pattern receptor Rig-I to promote efficient type I interferon production.** *Cell Microbiol* 2011, **13**(12):1907–1919.
230. Zhirnov OP, Konakova TE, Wolff T, Klenk HD: **NS1 protein of influenza A virus down-regulates apoptosis.** *J Virol* 2002, **76**(4):1617–1625.
231. Zhirnov OP, Klenk HD: **Control of apoptosis in influenza virus-infected cells by up-regulation of Akt and p53 signaling.** *Apoptosis* 2007, **12**(8):1419–1432.
232. Lu X, Masic A, Li Y, Shin Y, Liu Q, Zhou Y: **The PI3K/Akt pathway inhibits influenza A virus-induced Bax-mediated apoptosis by negatively regulating the JNK pathway via ASK1.** *J Gen Virol* 2010, **91**(Pt 6):1439–1449.
233. Obenauer JC, Denson J, Mehta PK, Su X, Mukatira S, Finkelstein DB, Xu X, Wang J, Ma J, Fan Y, *et al*: **Large-scale sequence analysis of avian influenza isolates.** *Science* 2006, **311**(5767):1576–1580.
234. Jackson D, Hossain MJ, Hickman D, Perez DR, Lamb RA: **A new influenza virus virulence determinant: the NS1 protein four C-terminal residues modulate pathogenicity.** *Proc Natl Acad Sci USA* 2008, **105**(11):4381–4386.
235. Zielecki F, Semmler I, Kalthoff D, Voss D, Mauel S, Gruber AD, Beer M, Wolff T: **Virulence determinants of avian H5N1 influenza A virus in mammalian and avian hosts: role of the C-terminal ESEV motif in the viral NS1 protein.** *J Virol* 2010, **84**(20):10708–10718.
236. Soubies SM, Volmer C, Croville G, Loupias J, Peralta B, Costes P, Lacroux C, Guerin JL, Volmer R: **Species-specific contribution of the four C-terminal amino acids of influenza A virus NS1 protein to virulence.** *J Virol* 2010, **84**(13):6733–6747.
237. Javier RT, Rice AP: **Emerging theme: cellular PDZ proteins as common targets of pathogenic viruses.** *J Virol* 2011, **85**(22):11544–11556.
238. Liu H, Golebiewski L, Dow EC, Krug RM, Javier RT, Rice AP: **The ESEV PDZ-binding motif of the avian influenza A virus NS1 protein protects infected cells from apoptosis by directly targeting Scribble.** *J Virol* 2010, **84**(21):11164–11174.
239. Golebiewski L, Liu H, Javier RT, Rice AP: **The Avian influenza NS1 ESEV PDZ binding motif associates with Dlg1 and scribble to disrupt cellular tight junctions.** *J Virol* 2011, **85**(20):10639–10648.
240. Thomas M, Kranjec C, Nagasaka K, Matlashewski G, Banks L: **Analysis of the PDZ binding specificities of Influenza A virus NS1 proteins.** *Virol J* 2011, **8**:25.
241. Qiu Y, Nemeroff M, Krug RM: **The influenza virus NS1 protein binds to a specific region in human U6 snRNA and inhibits U6-U2 and U6-U4 snRNA interactions during splicing.** *Rna* 1995, **1**(3):304–316.
242. Alonso-Caplen FV, Nemeroff ME, Qiu Y, Krug RM: **Nucleocytoplasmic transport: the influenza virus NS1 protein regulates the transport of spliced NS2 mRNA and its precursor NS1 mRNA.** *Genes Dev* 1992, **6**(2):255–267.
243. Qian XY, Alonso-Caplen F, Krug RM: **Two functional domains of the influenza virus NS1 protein are required for regulation of nuclear export of mRNA.** *J Virol* 1994, **68**(4):2433–2441.
244. Qiu Y, Krug RM: **The influenza virus NS1 protein is a poly(A)-binding protein that inhibits nuclear export of mRNAs containing poly(A).** *J Virol* 1994, **68**(4):2425–2432.
245. Noah DL, Twu KY, Krug RM: **Cellular antiviral responses against influenza A virus are countered at the posttranscriptional level by the viral NS1A protein via its binding to a cellular protein required for the 3' end processing of cellular pre-mRNAS.** *Virology* 2003, **307**(2):386–395.
246. Satterly N, Tsai PL, van Deursen J, Nussenzveig DR, Wang Y, Faria PA, Levay A, Levy DE, Fontoura BM: **Influenza virus targets the mRNA export machinery and the nuclear pore complex.** *Proc Natl Acad Sci USA* 2007, **104**(6):1853–1858.
247. Chen W, Calvo PA, Malide D, Gibbs J, Schubert U, Bacik I, Basta S, O'Neill R, Schickli J, Palese P, *et al*: **A novel influenza A virus mitochondrial protein that induces cell death.** *Nat Med* 2001, **7**(12):1306–1312.
248. Gibbs JS, Malide D, Hornung F, Bennink JR, Yewdell JW: **The influenza A virus PB1-F2 protein targets the inner mitochondrial membrane via a predicted basic amphipathic helix that disrupts mitochondrial function.** *J Virol* 2003, **77**(13):7214–7224.
249. Yamada H, Chounan R, Higashi Y, Kurihara N, Kido H: **Mitochondrial targeting sequence of the influenza A virus PB1-F2 protein and its function in mitochondria.** *FEBS Lett* 2004, **578**(3):331–336.
250. Zamarin D, Garcia-Sastre A, Xiao X, Wang R, Palese P: **Influenza virus PB1-F2 protein induces cell death through mitochondrial ANT3 and VDAC1.** *PLoS Pathog* 2005, **1**(1):e4.
251. Chanturiya AN, Basanez G, Schubert U, Henklein P, Yewdell JW, Zimmerberg J: **p B1–F2, an influenza A virus-encoded proapoptotic mitochondrial protein, creates variably sized pores in planar lipid membranes.** *J Virol* 2004, **78**(12):6304–6312.
252. Henkel M, Mitzner D, Henklein P, Meyer-Almes FJ, Moroni A, Difrancesco ML, Henkes LM, Kreim M, Kast SM, Schubert U, *et al*: **The proapoptotic influenza A virus protein PB1-F2 forms a nonselective ion channel.** *PLoS One* 2010, **5**(6):e11112.
253. McAuley JL, Chipuk JE, Boyd KL, Van De Velde N, Green DR, McCullers JA: **PB1-F2 proteins from H5N1 and 20 century pandemic influenza viruses cause immunopathology.** *PLoS Pathog* 2010, **6**(7):e1001014.
254. Varga ZT, Ramos I, Hai R, Schmolke M, Garcia-Sastre A, Fernandez-Sesma A, Palese P: **The influenza virus protein PB1-F2 inhibits the induction of type I interferon at the level of the MAVS adaptor protein.** *PLoS Pathog* 2011, **7**(6):e1002067.
255. Zamarin D, Ortigoza MB, Palese P: **Influenza A virus PB1-F2 protein contributes to viral pathogenesis in mice.** *J Virol* 2006, **80**(16):7976–7983.
256. McAuley JL, Hornung F, Boyd KL, Smith AM, McKeon R, Bennink J, Yewdell JW, McCullers JA: **Expression of the 1918 influenza A virus PB1-F2 enhances the pathogenesis of viral and secondary bacterial pneumonia.** *Cell Host Microbe* 2007, **2**(4):240–249.

257. Iverson AR, Boyd KL, McAuley JL, Plano LR, Hart ME, McCullers JA: **Influenza virus primes mice for pneumonia from Staphylococcus aureus.** *J Infect Dis* 2011, **203**(6):880–888.
258. Conenello GM, Zamarin D, Perrone LA, Tumpey T, Palese P: **A single mutation in the PB1-F2 of H5N1 (HK/97) and 1918 influenza A viruses contributes to increased virulence.** *PLoS Pathog* 2007, **3**(10):1414–1421.
259. Smith AM, Adler FR, McAuley JL, Gutenkunst RN, Ribeiro RM, McCullers JA, Perelson AS: **Effect of 1918 PB1-F2 expression on influenza A virus infection kinetics.** *PLoS Comput Biol* 2011, **7**(2):e1001081.
260. Mazur I, Anhlan D, Mitzner D, Wixler L, Schubert U, Ludwig S: **The proapoptotic influenza A virus protein PB1-F2 regulates viral polymerase activity by interaction with the PB1 protein.** *Cell Microbiol* 2008, **10**(5):1140–1152.
261. Haller O, Arnheiter H, Lindenmann J, Gresser I: **Host gene influences sensitivity to interferon action selectively for influenza virus.** *Nature* 1980, **283**(5748):660–662.
262. Staeheli P, Haller O, Boll W, Lindenmann J, Weissmann C: **Mx protein: constitutive expression in 3T3 cells transformed with cloned Mx cDNA confers selective resistance to influenza virus.** *Cell* 1986, **44**(1):147–158.
263. Haller O, Staeheli P, Kochs G: **Protective role of interferon-induced Mx GTPases against influenza viruses.** *Rev Sci Tech* 2009, **28**(1):219–231.
264. Haller O, Kochs G: **Interferon-induced mx proteins: dynamin-like GTPases with antiviral activity.** *Traffic* 2002, **3**(10):710–717.
265. Turan K, Mibayashi M, Sugiyama K, Saito S, Numajiri A, Nagata K: **Nuclear MxA proteins form a complex with influenza virus NP and inhibit the transcription of the engineered influenza virus genome.** *Nucleic Acids Res* 2004, **32**(2):643–652.
266. Dittmann J, Stertz S, Grimm D, Steel J, Garcia-Sastre A, Haller O, Kochs G: **Influenza A virus strains differ in sensitivity to the antiviral action of Mx-GTPase.** *J Virol* 2008, **82**(7):3624–3631.
267. Yount JS, Moltedo B, Yang YY, Charron G, Moran TM, Lopez CB, Hang HC: **Palmitoylome profiling reveals S-palmitoylation-dependent antiviral activity of IFITM3.** *Nat Chem Biol* 2010, **6**(8):610–614.
268. Wang X, Hinson ER, Cresswell P: **The interferon-inducible protein viperin inhibits influenza virus release by perturbing lipid rafts.** *Cell Host Microbe* 2007, **2**(2):96–105.
269. Kujime K, Hashimoto S, Gon Y, Shimizu K, Horie T: **p38 mitogen-activated protein kinase and c-jun-NH2-terminal kinase regulate RANTES production by influenza virus-infected human bronchial epithelial cells.** *J Immunol* 2000, **164**(6):3222–3228.
270. Ludwig S, Ehrhardt C, Neumeier ER, Kracht M, Rapp UR, Pleschka S: **Influenza virus-induced AP-1-dependent gene expression requires activation of the JNK signaling pathway.** *J Biol Chem* 2001, **276**(24):10990–10998.
271. Lin C, Zimmer SG, Lu Z, Holland RE Jr, Dong Q, Chambers TM: **The involvement of a stress-activated pathway in equine influenza virus-mediated apoptosis.** *Virology* 2001, **287**(1):202–213.
272. Maruoka S, Hashimoto S, Gon Y, Nishitoh H, Takeshita I, Asai Y, Mizumura K, Shimizu K, Ichijo H, Horie T: **ASK1 regulates influenza virus infection-induced apoptotic cell death.** *Biochem Biophys Res Commun* 2003, **307**(4):870–876.
273. Mori I, Goshima F, Koshizuka T, Koide N, Sugiyama T, Yoshida T, Yokochi T, Nishiyama Y, Kimura Y: **Differential activation of the c-Jun N-terminal kinase/stress-activated protein kinase and p38 mitogen-activated protein kinase signal transduction pathways in the mouse brain upon infection with neurovirulent influenza A virus.** *J Gen Virol* 2003, **84**(Pt 9):2401–2408.
274. Xing Z, Cardona CJ, Anunciacion J, Adams S, Dao N: **Roles of the ERK MAPK in the regulation of proinflammatory and apoptotic responses in chicken macrophages infected with H9N2 avian influenza virus.** *J Gen Virol* 2010, **91**(Pt 2):343–351.
275. Heynisch B, Frensing T, Heinze K, Seitz C, Genzel Y, Reichl U: **Differential activation of host cell signalling pathways through infection with two variants of influenza A/Puerto Rico/8/34 (H1N1) in MDCK cells.** *Vaccine* 2010, **28**(51):8210–8218.
276. Geiler J, Michaelis M, Sithisarn P, Cinatl J Jr: **Comparison of pro-inflammatory cytokine expression and cellular signal transduction in human macrophages infected with different influenza A viruses.** *Med Microbiol Immunol* 2011, **200**(1):53–60.
277. Ludwig S, Wolff T, Ehrhardt C, Wurzer WJ, Reinhardt J, Planz O, Pleschka S: **MEK inhibition impairs influenza B virus propagation without emergence of resistant variants.** *FEBS Lett* 2004, **561**(1–3):37–43.
278. Olschlager V, Pleschka S, Fischer T, Rziha HJ, Wurzer W, Stitz L, Rapp UR, Ludwig S, Planz O: **Lung-specific expression of active Raf kinase results in increased mortality of influenza A virus-infected mice.** *Oncogene* 2004, **23**(39):6639–6646.
279. Marjuki H, Gornitzky A, Marathe BM, Ilyushina NA, Aldridge JR, Desai G, Webby RJ, Webster RG: **Influenza A virus-induced early activation of ERK and PI3K mediates V-ATPase-dependent intracellular pH change required for fusion.** *Cell Microbiol* 2011, **13**(4):587–601.
280. De Clercq E: **Antiviral agents active against influenza A viruses.** *Nat Rev Drug Discov* 2006, **5**(12):1015–1025.
281. Ludwig S: **Disruption of virus-host cell interactions and cell signaling pathways as an anti-viral approach against influenza virus infections.** *Biol Chem* 2011, **392**(10):837–847.
282. Narayanan A, Bailey C, Kashanchi F, Kehn-Hall K: **Developments in antivirals against influenza, smallpox and hemorrhagic fever viruses.** *Expert Opin Investig Drugs* 2011, **20**(2):239–254.
283. Palmer R: **Drugs: lines of defence.** *Nature* 2011, **480**(7376):S9–10.
284. Fiore AE, Fry A, Shay D, Gubareva L, Bresee JS, Uyeki TM: **Antiviral agents for the treatment and chemoprophylaxis of influenza --- recommendations of the Advisory Committee on Immunization Practices (ACIP).** *MMWR Recomm Rep* 2011, **60**(1):1–24.
285. von Itzstein M, Wu WY, Kok GB, Pegg MS, Dyason JC, Jin B, Van Phan T, Smythe ML, White HF, Oliver SW, *et al*: **Rational design of potent sialidase-based inhibitors of influenza virus replication.** *Nature* 1993, **363**(6428):418–423.
286. Woods JM, Bethell RC, Coates JA, Healy N, Hiscox SA, Pearson BA, Ryan DM, Ticehurst J, Tilling J, Walcott SM, *et al*: **4-Guanidino-2,4-dideoxy-2,3-dehydro-N-acetylneuraminic acid is a highly effective inhibitor both of the sialidase (neuraminidase) and of growth of a wide range of influenza A and B viruses in vitro.** *Antimicrob Agents Chemother* 1993, **37**(7):1473–1479.
287. Kim CU, Lew W, Williams MA, Liu H, Zhang L, Swaminathan S, Bischofberger N, Chen MS, Mendel DB, Tai CY, *et al*: **Influenza neuraminidase inhibitors possessing a novel hydrophobic interaction in the enzyme active site: design, synthesis, and structural analysis of carbocyclic sialic acid analogues with potent anti-influenza activity.** *J Am Chem Soc* 1997, **119**(4):681–690.
288. Service RF: **Researchers seek new weapon against the flu.** *Science* 1997, **275**(5301):756–757.
289. Nguyen HT, Fry AM, Gubareva LV: **Neuraminidase inhibitor resistance in influenza viruses and laboratory testing methods.** *Antivir Ther* 2012, **17**(1 Pt B):159–173.
290. Birnkrant D, Cox E: **The Emergency Use Authorization of peramivir for treatment of 2009 H1N1 influenza.** *N Engl J Med* 2009, **361**(23):2204–2207.
291. Hernandez JE, Adiga R, Armstrong R, Bazan J, Bonilla H, Bradley J, Dretler R, Ison MG, Mangino JE, Maroushek S, *et al*: **Clinical experience in adults and children treated with intravenous peramivir for 2009 influenza A (H1N1) under an Emergency IND program in the United States.** *Clin Infect Dis* 2011, **52**(6):695–706.
292. Kiso M, Kubo S, Ozawa M, Le QM, Nidom CA, Yamashita M, Kawaoka Y: **Efficacy of the new neuraminidase inhibitor CS-8958 against H5N1 influenza viruses.** *PLoS Pathog* 2010, **6**(2):e1000786.
293. Furuta Y, Takahashi K, Kuno-Maekawa M, Sangawa H, Uehara S, Kozaki K, Nomura N, Egawa H, Shiraki K: **Mechanism of action of T-705 against influenza virus.** *Antimicrob Agents Chemother* 2005, **49**(3):981–986.
294. Kiso M, Takahashi K, Sakai-Tagawa Y, Shinya K, Sakabe S, Le QM, Ozawa M, Furuta Y, Kawaoka Y: **T-705 (favipiravir) activity against lethal H5N1 influenza A viruses.** *Proc Natl Acad Sci U S A* 2010, **107**(2):882–887.
295. Sleeman K, Mishin VP, Deyde VM, Furuta Y, Klimov AI, Gubareva LV: **In vitro antiviral activity of favipiravir (T-705) against drug-resistant influenza and 2009 A(H1N1) viruses.** *Antimicrob Agents Chemother* 2010, **54**(6):2517–2524.
296. Chan-Tack KM, Murray JS, Birnkrant DB: **Use of ribavirin to treat influenza.** *N Engl J Med* 2009, **361**(17):1713–1714.
297. Riner A, Chan-Tack KM, Murray JS: **Original research: Intravenous ribavirin–review of the FDA's Emergency Investigational New Drug Database (1997–2008) and literature review.** *Postgrad Med* 2009, **121**(3):139–146.
298. Su CY, Cheng TJ, Lin MI, Wang SY, Huang WI, Lin-Chu SY, Chen YH, Wu CY, Lai MM, Cheng WC, *et al*: **High-throughput identification of compounds targeting influenza RNA-dependent RNA polymerase activity.** *Proc Natl Acad Sci USA* 2010, **107**(45):19151–19156.
299. Kao RY, Yang D, Lau LS, Tsui WH, Hu L, Dai J, Chan MP, Chan CM, Wang P, Zheng BJ, *et al*: **Identification of influenza A nucleoprotein as an antiviral target.** *Nat Biotechnol* 2010, **28**(6):600–605.

300. Gerritz SW, Cianci C, Kim S, Pearce BC, Deminie C, Discotto L, McAuliffe B, Minassian BF, Shi S, Zhu S, *et al*: Inhibition of influenza virus replication via small molecules that induce the formation of higher-order nucleoprotein oligomers. *Proc Natl Acad Sci USA* 2011, 108(37):15366–15371.
301. Amorim MJ, Kao RY, Digard P: Nucleozin targets cytoplasmic trafficking of viral ribonucleoprotein-Rab11 complexes in influenza A virus infection. *J Virol* 2013, 87(8):4694–4703.
302. Jablonski JJ, Basu D, Engel DA, Geysen HM: Design, synthesis, and evaluation of novel small molecule inhibitors of the influenza virus protein NS1. *Bioorg Med Chem* 2012, 20(1):487–497.
303. Basu D, Walkiewicz MP, Frieman M, Baric RS, Auble DT, Engel DA: Novel influenza virus NS1 antagonists block replication and restore innate immune function. *J Virol* 2009, 83(4):1881–1891.
304. Walkiewicz MP, Basu D, Jablonski JJ, Geysen HM, Engel DA: Novel inhibitor of influenza non-structural protein 1 blocks multi-cycle replication in an RNase L-dependent manner. *J Gen Virol* 2011, 92(Pt 1):60–70.
305. Brooks MJ, Burtseva EI, Ellery PJ, Marsh GA, Lew AM, Slepushkin AN, Crowe SM, Tannock GA: Antiviral activity of arbidol, a broad-spectrum drug for use against respiratory viruses, varies according to test conditions. *J Med Virol* 2012, 84(1):170–181.
306. Taylor HP, Dimmock NJ: Competitive binding of neutralizing monoclonal and polyclonal IgG to the HA of influenza A virions in solution: only one IgG molecule is bound per HA trimer regardless of the specificity of the competitor. *Virology* 1994, 205(1):360–363.
307. Taylor HP, Armstrong SJ, Dimmock NJ: Quantitative relationships between an influenza virus and neutralizing antibody. *Virology* 1987, 159(2):288–298.
308. Sui J, Hwang WC, Perez S, Wei G, Aird D, Chen LM, Santelli E, Stec B, Cadwell G, Ali M, *et al*: Structural and functional bases for broad-spectrum neutralization of avian and human influenza A viruses. *Nat Struct Mol Biol* 2009, 16(3):265–273.
309. Tamura M, Webster RG, Ennis FA: Neutralization and infection-enhancement epitopes of influenza A virus hemagglutinin. *J Immunol* 1993, 151(3):1731–1738.
310. Yewdell JW, Taylor A, Yellen A, Caton A, Gerhard W, Bachi T: Mutations in or near the fusion peptide of the influenza virus hemagglutinin affect an antigenic site in the globular region. *J Virol* 1993, 67(2):933–942.
311. Virelizier JL: Host defenses against influenza virus: the role of anti-hemagglutinin antibody. *J Immunol* 1975, 115(2):434–439.
312. Barbey-Martin C, Gigant B, Bizebard T, Calder LJ, Wharton SA, Skehel JJ, Knossow M: An antibody that prevents the hemagglutinin low pH fusogenic transition. *Virology* 2002, 294(1):70–74.
313. Ekiert DC, Bhabha G, Elsliger MA, Friesen RH, Jongeneelen M, Throsby M, Goudsmit J, Wilson IA: Antibody recognition of a highly conserved influenza virus epitope. *Science* 2009, 324(5924):246–251.
314. Knossow M, Gaudier M, Douglas A, Barrère B, Bizebard T, Barbey C, Gigant B, Skehel JJ: Mechanism of neutralization of influenza virus infectivity by antibodies. *Virology* 2002, 302(2):294–298.
315. Chan RW, Chan MC, Wong AC, Karamanska R, Dell A, Haslam SM, Sihoe AD, Chui WH, Triana-Baltzer G, Li Q, *et al*: DAS181 inhibits H5N1 influenza virus infection of human lung tissues. *Antimicrob Agents Chemother* 2009, 53(9):3935–3941.
316. Triana-Baltzer GB, Gubareva LV, Klimov AI, Wurtman DF, Moss RB, Hedlund M, Larson JL, Belshe RB, Fang F: Inhibition of neuraminidase inhibitor-resistant influenza virus by DAS181, a novel sialidase fusion protein. *PLoS One* 2009, 4(11):e7838.
317. Triana-Baltzer GB, Gubareva LV, Nicholls JM, Pearce MB, Mishin VP, Belser JA, Chen LM, Chan RW, Chan MC, Hedlund M, *et al*: Novel pandemic influenza A(H1N1) viruses are potently inhibited by DAS181, a sialidase fusion protein. *PLoS One* 2009, 4(11):e7788.
318. Zhirnov OP, Ovcharenko AV, Bukrinskaya AG: Suppression of influenza virus replication in infected mice by protease inhibitors. *J Gen Virol* 1984, 65(Pt 1):191–196.
319. Bottcher-Friebertshauser E, Freuer C, Sielaff F, Schmidt S, Eickmann M, Uhlendorff J, Steinmetzer T, Klenk HD, Garten W: Cleavage of influenza virus hemagglutinin by airway proteases TMPRSS2 and HAT differs in subcellular localization and susceptibility to protease inhibitors. *J Virol* 2010, 84(11):5605–5614.
320. Sielaff F, Bottcher-Friebertshauser E, Meyer D, Saupe SM, Volk IM, Garten W, Steinmetzer T: Development of substrate analogue inhibitors for the human airway trypsin-like protease HAT. *Bioorg Med Chem Lett* 2011, 21(16):4860–4864.
321. Droebner K, Pleschka S, Ludwig S, Planz O: Antiviral activity of the MEK-inhibitor U0126 against pandemic H1N1v and highly pathogenic avian influenza virus in vitro and in vivo. *Antivir Res* 2011, 92(2):195–203.
322. Mazur I, Wurzer WJ, Ehrhardt C, Pleschka S, Puthavathana P, Silberzahn T, Wolff T, Planz O, Ludwig S: Acetylsalicylic acid (ASA) blocks influenza virus propagation via its NF-kappaB-inhibiting activity. *Cell Microbiol* 2007, 9(7):1683–1694.
323. Starko KM: Salicylates and pandemic influenza mortality, 1918–1919 pharmacology, pathology, and historic evidence. *Clin Infect Dis* 2009, 49(9):1405–1410.
324. Eyers S, Weatherall M, Shirtcliffe P, Perrin K, Beasley R: The effect on mortality of antipyretics in the treatment of influenza infection: systematic review and meta-analysis. *J R Soc Med* 2010, 103(10):403–411.
325. Marsolais D, Hahm B, Walsh KB, Edelmann KH, McGavern D, Hatta Y, Kawaoka Y, Rosen H, Oldstone MB: A critical role for the sphingosine analog AAL-R in dampening the cytokine response during influenza virus infection. *Proc Natl Acad Sci USA* 2009, 106(5):1560–1565.
326. Walsh KB, Teijaro JR, Wilker PR, Jatzek A, Fremgen DM, Das SC, Watanabe T, Hatta M, Shinya K, Suresh M, *et al*: Suppression of cytokine storm with a sphingosine analog provides protection against pathogenic influenza virus. *Proc Natl Acad Sci USA* 2011, 108(29):12018–12023.
327. Liu Y-Y, Slotine J-J, Barabási A-L: Controllability of complex networks. *Nature* 2011, 473(7346):167–173.
328. Luni C, Shoemaker JE, Sanft KR, Petzold LR, Doyle FJ 3rd: Confidence from uncertainty–a multi-target drug screening method from robust control theory. *BMC Syst Biol* 2010, 4:161.
329. Kotlyar M, Fortney K, Jurisica I: Network-based characterization of drug-regulated genes, drug targets, and toxicity. *Methods* 2012, 57(4):499–507.
330. Cameron CM, Cameron MJ, Bermejo-Martin JF, Ran L, Xu L, Turner PV, Ran R, Danesh A, Fang Y, Chan PK, *et al*: Gene expression analysis of host innate immune responses during Lethal H5N1 infection in ferrets. *J Virol* 2008, 82(22):11308–11317.
331. Cilloniz C, Shinya K, Peng X, Korth MJ, Proll SC, Aicher LD, Carter VS, Chang JH, Kobasa D, Feldmann F, *et al*: Lethal influenza virus infection in macaques is associated with early dysregulation of inflammatory related genes. *PLoS Pathog* 2009, 5(10):e1000604.
332. Cilloniz C, Pantin-Jackwood MJ, Ni C, Goodman AG, Peng X, Proll SC, Carter VS, Rosenzweig ER, Szretter KJ, Katz JM, *et al*: Lethal dissemination of H5N1 influenza virus is associated with dysregulation of inflammation and lipoxin signaling in a mouse model of infection. *J Virol* 2010, 84(15):7613–7624.
333. Li C, Bankhead A 3rd, Eisfeld AJ, Hatta Y, Jeng S, Chang JH, Aicher LD, Proll S, Ellis AL, Law GL, *et al*: Host regulatory network response to infection with highly pathogenic H5N1 avian influenza virus. *J Virol* 2011, 85(21):10955–10967.

doi:10.1186/1752-0509-7-97
Cite this article as: Matsuoka *et al.*: A comprehensive map of the influenza A virus replication cycle. *BMC Systems Biology* 2013 7:97.

Submit your next manuscript to BioMed Central and take full advantage of:

- Convenient online submission
- Thorough peer review
- No space constraints or color figure charges
- Immediate publication on acceptance
- Inclusion in PubMed, CAS, Scopus and Google Scholar
- Research which is freely available for redistribution

Submit your manuscript at
www.biomedcentral.com/submit

BioMed Central

OPEN ACCESS Freely available online

PLOS ONE

Modeling of Rifampicin-Induced CYP3A4 Activation Dynamics for the Prediction of Clinical Drug-Drug Interactions from *In Vitro* Data

Fumiyoshi Yamashita[1]*, Yukako Sasa[1], Shuya Yoshida[1], Akihiro Hisaka[2], Yoshiyuki Asai[3], Hiroaki Kitano[3,4], Mitsuru Hashida[1,5], Hiroshi Suzuki[6]

1 Department of Drug Delivery Research, Graduate School of Pharmaceutical Sciences, Kyoto University, Kyoto, Japan, **2** Department of Pharmacology and Pharmacokinetics, The University of Tokyo Hospital, Faculty of Medicine, The University of Tokyo, Tokyo, Japan, **3** Open Biology Unit, Okinawa Institute of Science and Technology Graduate University, Okinawa, Japan, **4** Sony Computer Science Laboratories, Inc, Tokyo, Japan, **5** Institute for Integrated Cell-Material Sciences, Kyoto University, Kyoto, Japan, **6** Department of Pharmacy, The University of Tokyo Hospital, Faculty of Medicine, The University of Tokyo, Tokyo, Japan

Abstract

Induction of cytochrome P450 3A4 (CYP3A4) expression is often implicated in clinically relevant drug-drug interactions (DDI), as metabolism catalyzed by this enzyme is the dominant route of elimination for many drugs. Although several DDI models have been proposed, none have comprehensively considered the effects of enzyme transcription/translation dynamics on induction-based DDI. Rifampicin is a well-known CYP3A4 inducer, and is commonly used as a positive control for evaluating the CYP3A4 induction potential of test compounds. Herein, we report the compilation of *in vitro* induction data for CYP3A4 by rifampicin in human hepatocytes, and the transcription/translation model developed for this enzyme using an extended least squares method that can account for inherent inter-individual variability. We also developed physiologically based pharmacokinetic (PBPK) models for the CYP3A4 inducer and CYP3A4 substrates. Finally, we demonstrated that rifampicin-induced DDI can be predicted with reasonable accuracy, and that a static model can be used to simulate DDI once the blood concentration of the inducer reaches a steady state following repeated dosing. This dynamic PBPK-based DDI model was implemented on a new multi-hierarchical physiology simulation platform named PhysioDesigner.

Citation: Yamashita F, Sasa Y, Yoshida S, Hisaka A, Asai Y, et al. (2013) Modeling of Rifampicin-Induced CYP3A4 Activation Dynamics for the Prediction of Clinical Drug-Drug Interactions from *In Vitro* Data. PLoS ONE 8(9): e70330. doi:10.1371/journal.pone.0070330

Editor: Randen Lee Patterson, UC Davis School of Medicine, United States of America

Received February 28, 2013; **Accepted** June 17, 2013; **Published** September 24, 2013

Copyright: © 2013 Yamashita et al. This is an open-access article distributed under the terms of the Creative Commons Attribution License, which permits unrestricted use, distribution, and reproduction in any medium, provided the original author and source are credited.

Funding: This research was supported in part by Grant-in-Aid for Scientific Research on Innovative Areas (23136102) from the Ministry of Education, Culture, Sports, Science and Technology, Japan (http://www.mext.go.jp/). The funders had no role in study design, data collection and analysis, decision to publish, or preparation of the manuscript.

Competing Interests: Co-author HK is a president and CEO at Sony Computer Science Laboratories, Inc., Tokyo, Japan. There are no patents, products in development or marketed products to declare. This does not alter the authors' adherence to all the PLOS ONE policies on sharing data and materials.

* E-mail: yama@pharm.kyoto-u.ac.jp

Introduction

Cytochrome P450 enzymes (CYPs) are implicated in many clinically relevant drug-drug interactions (DDI), as the metabolism reactions catalyzed by this enzyme family are the dominant route of elimination for the majority of drugs. Inhibition of the CYPs can lead to an unwanted elevation in the blood level of drugs administered concomitantly, which can result in life-threatening adverse drug reactions [1,2]. Induction of CYP expression is not normally considered to be a safety concern, but can lead to inadequate drug efficacy [3]. For example, co-administration of rifampicin and cyclosporine results in excess metabolism of cyclosporine leading to allograft rejection in transplanted patients [4–6]. Thus, predictions of *in vivo* DDIs from *in vitro* metabolism data are becoming increasingly important during the process of preclinical drug development.

Various mathematical models have been proposed to predict potential clinical drug-drug interactions from *in vitro* data [7–10]. However, induction studies are generally more difficult to conduct compared with inhibition studies, as they need a cell-based system that allows evaluation of gene transcription and protein expression. The simplest model is one in which a static score of degree of induction is calculated from the average plasma concentration of an inducer using *in vitro* EC_{50} and E_{max} estimates [11,12]. The potential for induction-based DDI for any particular drug combination is then predicted based on the proportion of the drugs' total body clearance attributable to the enzymes induced. Dynamic models consider fluctuations in the levels of enzyme activity [13–15]. The clearance rate of substrate drugs can be dynamically altered by the acceleration of enzyme synthesis in an inducer concentration-dependent manner. A recent study indicated that a dynamic model, although not a marked improvement over the static model, tended to give better predictions for the 50 clinical DDI cases studied [16].

To date, the dynamic models reported are all indirect pharmacokinetic/pharmacodynamic (PK/PD) models [13–15] which assume that an inducer accelerates the enzyme synthesis in a concentration-dependent manner. Since enzyme synthesis is assumed to obey zero-order kinetics, the action of the inducer on enzyme synthesis starts immediately. Therefore, the gradual increase in CYP activity over several days' exposure to the inducer is attributed simply to the slow degradation rate of these

enzymes. However, several studies have indicated that it takes at least a few days for the mRNA to reach a maximum level [17,18]. To evaluate the kinetics of enzyme induction, it is important to consider the time courses of sequential mRNA and enzyme synthesis.

The present study is aimed at developing a hybrid simulation model for predicting the dynamics of induction-based DDI, in which a whole-body physiologically based pharmacokinetic (PBPK) model and an enzyme transcription/translation dynamics model are implemented. Feasibility of this hybrid model was investigated using rifampicin, a well-characterized and potent inducer of CYP3A4. Rifampicin is frequently used as a positive control or calibrator for evaluating the CYP3A4 induction potential of test compounds. Therefore, a large amount of *in vitro* rifampicin data is available in the literature. In general, cultures of primary human hepatocytes are believed to be the best *in vitro* model for simulating *in vivo* conditions. However, considerable functional variability of donor hepatocytes has been observed [19,20]. To obtain non-biased parameters regarding transcription and translation of CYP3A4, we systematically collected *in vitro* data and analyzed them using an extended least squares method [21,22] that allows the estimation of kinetic parameters while taking inter- and intra-individual variability into account. Using the parameters estimated from *in vitro* human hepatocytes, we then predicted clinical pharmacokinetics of CYP3A4 substrate drugs in the presence of concomitantly administered rifampicin.

Materials and Methods

Data Collection

The fm_{CYP3A4} values, i.e., the apparent contribution of CYP3A4 to drug oral clearance, were obtained for 15 CYP3A4 substrate drugs in a previous report [23,24]. These values were estimated from the increase in AUC_{oral} of the drugs tested resulting from the action of CYP3A4 inhibitors, as observed in 53 separate clinical DDI studies [23]. AUC_{oral} is the area under the blood concentration-time profile following oral administration. Information on the pharmacokinetics of CYP3A4 substrate drugs when co-administered with rifampicin (see Table S1) was also obtained from the literature [25–40]. The dosage regimen of oral rifampicin was also considered in the present analysis. Clinical pharmacokinetic data of rifampicin with different oral dosage regimens were obtained from a report by Acocella et al. [41]. In addition, *in vitro* rifampicin induction data of CYP3A4 mRNA expression and/or enzyme activity in primary cultures of human hepatocytes were also collected [17,42–46].

Modeling of the induction dynamics of CYP3A4 expression in human hepatocytes

Following the onset of treatment of hepatocytes with rifampicin, expression of CYP3A4 mRNA was up-regulated after an initial time delay, and reached maximum level on day 2 [17]. Taking into account that rifampicin induces expression of CYP3A4 via activation of the pregnane X receptor (PXR), a dynamic model with a putative receptor was defined using the following equations:

$$\frac{dPXR_{act}}{dt} = \frac{1+CYP_0/K_i}{1+CYP/K_i}\cdot\frac{RIF}{EC_{50}+RIF} - k_{inact}\cdot PXR_{act} \quad (1)$$

$$\frac{dRNA}{dt} = k_{rna,syn} + k_{rna,pxr}\cdot PXR_{act} - k_{\mathrm{rna,deg}}\cdot RNA \quad (2)$$

$$\frac{dCYP}{dt} = k_{cyp,syn}\cdot RNA - k_{\mathrm{cyp,deg}}\cdot CYP \quad (3)$$

where RIF, PXR_{act}, RNA, and CYP are the concentration of rifampicin, normalized amount of activated PXR, CYP3A4 mRNA level, and CYP3A4 enzyme level, respectively, CYP_0, EC_{50}, K_i, and k_{inact} are the baseline level of CYP3A4 enzyme, concentration of rifampicin at half-maximum PXR activation, the constant for negative feedback inhibition, and the inactivation rate constant for activated PXR, respectively. $k_{rna,syn}$ and $k_{rna,pxr}$ are rate constants for baseline and PXR-mediated synthesis of CYP3A4 mRNA, and $k_{rna,deg}$ is the rate constant for its sequestration, while $k_{cyp,syn}$ and $k_{cyp,deg}$ are rate constants for the synthesis and sequestration of CYP3A4 enzyme. In the model, a delay in the early phase of CYP3A4 mRNA expression after addition of the inducer was assumed to be attributable to the time required for activation of PXR, while the accelerated decay of this mRNA was thought to result from the subsequent negative feedback inhibition by PXR according to CYP3A4 level. In general, induction of mRNA and subsequent CYP3A4 enzyme levels is evaluated as the fold increase over the value observed on day 0. If the levels of mRNA and enzyme return to their original values (RNA_0 and CYP_0, respectively) by the removal of a stimulus, the following relationships should be satisfied:

$$k_{cyp,syn}\cdot RNA_0 = k_{\mathrm{cyp,deg}}\cdot CYP_0 \quad (4)$$

$$k_{rna,syn} = k_{\mathrm{rna,deg}}\cdot RNA_0 \quad (5)$$

Therefore, using $RNA' = RNA/\mathrm{RNA}_0$ and $CYP' = CYP/CYP_0$, Eqs. 1–3 can be replaced with:

$$\frac{dPXR_{act}}{dt} = \frac{1+p}{1+p\cdot CYP'}\cdot\frac{RIF}{EC_{50}+RIF} - k_{inact}\cdot PXR_{act} \quad (6)$$

$$\frac{dRNA'}{dt} = k_{\mathrm{rna,deg}}\cdot(1+q\cdot PXR_{act} - RNA') \quad (7)$$

$$\frac{dCYP'}{dt} = k_{cyp,\mathrm{deg}}\cdot(RNA' - CYP') \quad (8)$$

where

$$p = CYP_0/Ki \quad (9)$$

$$q = \frac{k_{rna,pxr}\cdot k_{\mathrm{cyp,syn}}}{k_{rna,\mathrm{deg}}\cdot k_{\mathrm{cyp,deg}}\cdot CYP_0} \quad (10)$$

Since the considerable inter-donor variability of drug metabolism by human hepatocytes has been attributed to variations in the baseline level of the CYP3A4 activity present [20], an extended least square analysis was performed by considering the effect of inter-donor variability on CYP_0 (that is, p and q). This analysis was carried out using the ADVAN9 routine in NONMEM 7.2 (Icon, Inc., Dublin, Ireland).

Conventional modeling of the induction dynamics of CYP3A4 activity

An indirect effect model for enzyme induction [13–15] can be represented as follows:

$$\frac{dCYP}{dt} = k_{syn} \cdot \left(1 + \frac{E_{\max} \cdot RIF}{EC_{50} + RIF}\right) - k_{\deg} \cdot CYP \qquad (11)$$

where k_{syn} and k_{deg} are rate constants for baseline synthesis and sequestration of CYP3A4 enzyme, respectively. Assuming that the level of enzyme prior to administration of rifampicin (CYP_0) was under the steady state, the following relationship should be satisfied:

$$k_{syn} = k_{\deg} \cdot CYP_0 \qquad (12)$$

Replacing the k_{syn} of Eq. 11 and normalizing it with CYP_0 ($CYP' = CYP/CYP_0$), we obtain:

$$\frac{dCYP'}{dt} = k_{\deg} \cdot \left(1 + \frac{E_{\max} \cdot RIF}{EC_{50} + RIF} - CYP'\right) \qquad (13)$$

An extended least square analysis was performed by considering the effect of inter-donor variability on E_{max}. This analysis was carried out using the ADVAN9 routine in NONMEM 7.2.

Analysis of CYP3A4 activity induction by a simple static model

Using only 72-h data, the E_{max} and EC_{50} values for induction of CYP3A4 by rifampicin were estimated from the following equation:

$$CYP' = 1 + \frac{E_{\max} \cdot RIF}{EC_{50} + RIF} \qquad (14)$$

An extended least square analysis was performed by considering the effect of inter-donor variability on E_{max}, similarly to the case of the indirect effect model mentioned before.

Modeling of the clinical pharmacokinetics of rifampicin following repeated oral dosing

PBPK models are mechanistically rigorous models that incorporate anatomical and biochemical information into descriptions of pharmacokinetics. To construct PBPK models, measurements of drug concentrations in each organ and tissue are required. However, only blood and urine data are generally available in clinic. As an intermediate approach, a PBPK model which gives an abstracted blood compartment and considers only recirculation between blood and liver has been utilized [7]. It has been demonstrated that the simplified PBPK model allows *in vitro-in vivo* extrapolation of hepatic drug metabolism [7]. Rifampicin clearance is known to be a nonlinear saturable process that accelerates during repeated oral dosing [41]. The simplified PBPK model was modified taking this specialized aspect of rifampicin pharmacokinetics into consideration. The mass-balance equations were:

$$V_1 \frac{dC_b}{dt} = -Q_h \cdot C_b + Q_h \cdot \frac{C_h \cdot R_b}{K_{p,h}} - CL_r \cdot C_b \qquad (15)$$

$$V_h \cdot \frac{dC_h}{dt} = Q_h \cdot C_b - Q_h \cdot \frac{C_h \cdot R_b}{K_{p,h}} - \frac{V_{\max} \cdot fu_p \cdot C_h / K_{p,h}}{K_m + fu_p \cdot C_h / K_{p,h}} + \sum^{t_i < t} k_a \cdot F_a F_g \cdot D \cdot \delta(t_i) \cdot \exp(-k_a \cdot (t - t_i)) \qquad (16)$$

$$\frac{dV_{\max}}{dt} = k_{in} \cdot (1 + F \cdot fu_p \cdot C_h / K_{p,h}) - k_{out} \cdot V_{\max} \qquad (17)$$

where C_b and C_h are concentrations of the drug in the blood and liver, respectively, and V_{max} is the inducible maximum hepatic elimination rate. V_1, CL_r, Q_h, R_b, and $K_{p,h}$ are the volume of systemic circulation, renal clearance, hepatic plasma flow rate, blood/plasma distribution ratio, and liver/plasma distribution ratio, respectively. V_h, fu_p, K_m, k_a, F_aF_g, and D are the volume of liver, fraction unbound in plasma, Michaelis-Menten constant for hepatic elimination, absorption rate constant, product of fraction absorbed and intestinal availability, and amount of oral dose, respectively. k_{in}, k_{out}, and F are the rate constant for synthesis of hepatic elimination activity, rate constant for decay of hepatic elimination activity, and coefficient for auto-induction, respectively. CL_r and fu_p were assumed to be 1.8 L/h and 0.2 [47], respectively. Q_h and V_h were assumed to be 96.6 L/h and 1.4 L, respectively [7]. Assuming that F_aF_g and R_b were both at unity, V_1, K_m, k_a, $K_{p,h}$, k_{in}, k_{out}, and F were estimated by curve-fitting to blood concentration-time profiles following repeated oral dosing of rifampicin with different doses [41]. The parameter estimation procedure was carried out with the ADVAN9 routine in NONMEM 7.2.

Simulation of drug-drug interactions with rifampicin

In the case of drugs that are mostly metabolized by the liver, induction-based DDI occurring after oral administration is represented by:

$$\frac{AUC^{ind}}{AUC} = \frac{1}{fm_{CYP3A4} \cdot IR + (1 - fm_{CYP3A4})} \qquad (18)$$

where AUC and AUC^{ind} are areas under the blood concentration profile in the absence and presence of an inducer, respectively. fm_{CYP3A4} and IR are the fraction of the drug metabolized by CYP3A4 and the relative activity of CYP3A4 induced by the inducer, respectively. This equation has been derived using the following assumptions: the substrate drug is eliminated solely by the liver, and the induction of CYP3A4 in the intestine is negligible. The fm_{CYP3A4} values for each substrate drug were obtained from the literature [23,24]. In the previous article [24], 53 induction-based DDI data sets in human were collected and compiled without any normalization, demonstrating that the degree of DDIs could be comprehensively explained by the IR values of various inducers determined from *in vivo* data by taking simvastatin as a standard CYP3A4 substrate. In the present study, only data for rifampicin were taken from the compiled data. The IR value for rifampicin was estimated using *in vitro* parameters with the following process: Using Eqs. 15–17, the unbound concentration of rifampicin in the liver ($fu_p \cdot C_h / K_{p,h}$) was computed. By substituting it for the variable RIF in Eq. 6 or 13, a time-course for the degree of induction of CYP3A4 (CYP') *in vivo* was estimated by Eqs. 6–8 or Eq. 13. The IR was defined as the average of CYP' over the interval.

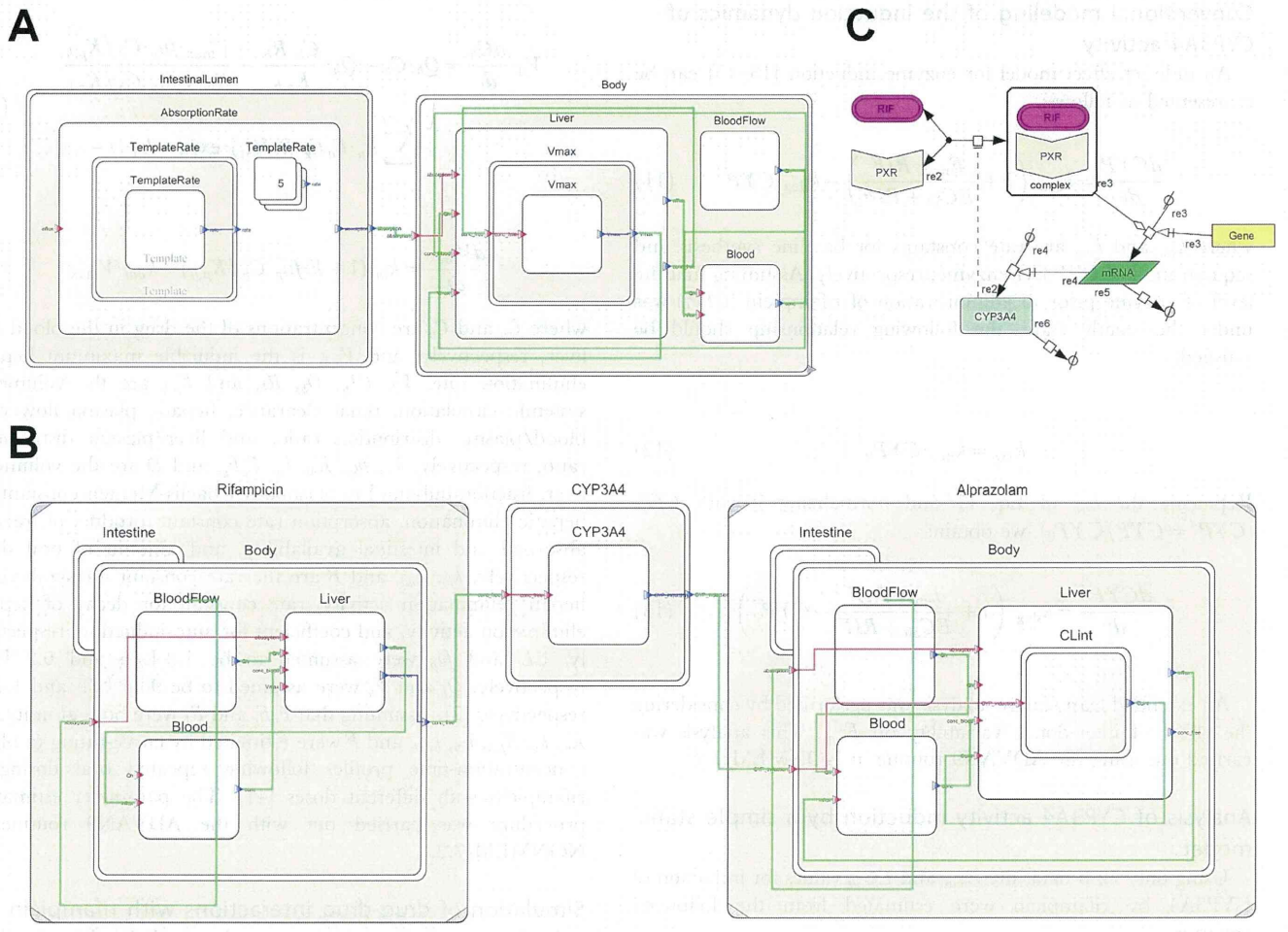

Figure 1. Snapshots of DDI models implemented in multi-hierarchical physiology simulation platforms. Fig. 1A represents a PBPK model for rifampicin implemented on PhysioDesigner, and Fig. 1B represents a transcription/translation dynamics model for CYP3A4 following administration of the drug, as implemented on CellDesigner. Fig. 1C represents a PBPK-based DDI model, where the enzyme induction model was hybridized. Yellow and white rectangles represent the capsule module and functional module, respectively. Modules can communicate by connecting their ports with an edge.
doi:10.1371/journal.pone.0070330.g001

To simulate the blood concentration-time profile of a CYP3A4 substrate drug in the presence of rifampicin, a PBPK model for the substrate, similar to that for rifampicin (Eqs. 15–17), was considered. Assuming that hepatic elimination is linear, the mass-balance equation for the liver was replaced with:

$$V_h \cdot \frac{dC_h}{dt} = Q_h \cdot C_b - Q_h \cdot \frac{C_h \cdot R_b}{K_{p,h}} - CL_{\mathrm{int},h} \cdot fu_p \cdot C_h / K_{p,h} + \sum_{t_i < t} k_a \cdot F_a F_g \cdot D \cdot \delta(t_i) \cdot \exp(-k_a \cdot (t - t_i)) \quad (19)$$

where $CL_{int,h}$ depicts intrinsic clearance for the substrate. Pharmacokinetic parameters for CYP3A4 substrates were obtained by curve-fitting to their blood concentration profiles as has been reported previously [7]. For simulation of DDI with rifampicin, $CL_{int,h}$ was assumed to be dependent on CYP':

$$CL^{ind}_{\mathrm{int},h} = CL^{0}_{\mathrm{int},h} \cdot (fm_{CYP3A4} \cdot CYP' + (1 - fm_{CYP3A4})) \quad (20)$$

where $CL^{ind}_{\mathrm{int},h}$ and $CL^{0}_{\mathrm{int},h}$ are intrinsic clearances for the substrate in the presence and absence of rifampicin, respectively. Thus, two PBPK models for the inducer and substrate were bridged with the CYP3A4 induction dynamics model to compute the DDI with rifampicin.

PHML-SBML hybrid simulation

Physiological Hierarchy Markup Language (PHML) is a markup language that can explicitly describe the multi-level hierarchical structures of physiological functions in mathematical models. One of the remarkable features of PHML is that it enables the embedding of Systems Biology Markup Language (SBML) [48] models as a module. To make a DDI model more readable and reusable, two PBPK models for both inducer and substrate were stored in the PHML format, and connected to each other via a functional module representing subcellular enzyme induction, of which the contents were implemented in SBML. The PHML and SBML models were developed using open source modeling platforms, PhysioDesigner (formerly *insilico*IDE) and CellDesigner, respectively [49,50]. PhysioDesigner and CellDesigner are freely available at http://physiodesigner.org and http://celldesigner.org.

Fig. 1 represents snapshots of the DDI model implemented in the simulation platform. As shown in Fig. 1A, a PBPK model is

primarily composed of two modules corresponding to the intestinal lumen and body. Between these modules, it is enough to pass only the value of an intestinal drug absorption rate. To ensure maintainability and scalability of the model, these modules were capsuled to hide unnecessary values, and opened with only a port to pass the absorption rate value. By connecting the ports with an edge, these capsule modules can communicate with each other. Each module was further modeled in a hierarchical manner. Using a template/instance framework of PHML, the absorption rate was calculated in the intestinal lumen module by summing up the values from each of the instances corresponding to multiple doses. The body module includes the functional modules for the liver and blood, in addition to a module for common static variables. Differential equations and variables were implemented in the liver and blood modules. Upon developing PBPK models for an inducer and a CYP3A4 substrate drug, the models were bridged with a capsuled functional module for induction of CYP3A4 (Fig. 1B). The CYP3A4 induction module receives the unbound concentration of the inducer in the liver from the inducer PBPK model and provides the *IR* value for the substrate PBPK model. However, the module was simply a frame, and its object was implemented in a SBML format. Fig. 1C represents a SBML model for induction of CYP3A4 developed using CellDesigner.

Results

Modeling of CYP induction dynamics

The pooled data set obtained from 24 different sources comprised 43 and 40 data points for CYP3A4 enzyme activity and mRNA expression levels, respectively. Considering the effect of inter-donor variability on the baseline level of CYP3A4 activity, an extended least square analysis was performed based on Eqs. 6–8 (see Methods). The parameters EC_{50}, k_{inact}, $k_{rna,deg}$, $k_{cyp,deg}$, p and q were estimated to be 1.18 μM, 0.0530 h^{-1}, 0.0282 h^{-1}, 0.313, and 4.34, respectively, in addition to the inter-donor variability of CYP_0 (ω^2) of 0.318. Interestingly, the $k_{cyp,deg}$ estimated was comparable to the one that was previously optimized for better *in vitro/in vivo* extrapolation (0.03 h^{-1}) [51,52]. Fig. 2 represents simulated surface plots for mean CYP3A4 activity and mRNA expression as a function of concentration and time. Expression of mRNA reached a maximum level at ~40 h following the onset of incubation with rifampicin, whereas the peak of CYP3A4 activity induction was delayed in comparison.

The data set for induction of CYP3A4 activity was also analyzed based on a conventionally used indirect effect model. However, simultaneous estimation of all parameters by curve fitting failed, probably because estimation of k_{deg} requires a clear observation of the maximally induced state in the profile. Alternatively, using the k_{deg} value from the literature [51,52], the EC_{50} and E_{max} values were estimated by curve-fitting. When the k_{deg} value was a default value of the Symcyp simulator (0.0072 h^{-1}), the EC_{50} and E_{max} values were estimated to be 0.283 μM and 37.1, respectively, in addition to a ω_{Emax}^2 of 0.726. When the k_{deg} corrected for more accurate *in vitro-in vivo* extrapolation (0.03 h^{-1}) [51,52] was used, the EC_{50} and E_{max} values were estimated to be 0.269 μM and 16.7, respectively, in addition to a ω_{Emax}^2 of 0.702.

When the analysis based on a simple static model was performed using only 72-h data, the EC_{50} and E_{max} values were estimated to be 0.281 μM and 14.8, respectively. The ω_{Emax}^2 value was 0.874.

Modeling of the clinical pharmacokinetics of rifampicin

Blood concentration-time profiles following repeated oral administration of rifampicin were simultaneously analyzed to estimate its pharmacokinetic parameters based on a simplified PBPK model. The estimated k_a, V_1, K_m, $K_{p,h}$, k_{in}, k_{out}, and F values were 0.963 h^{-1}, 17.2 L, 0.370 mg/L, 10.6, 0.0193 mg/h, 5.75×10^{-4} h^{-1}, and 8.64 L/mg, respectively. Fig. 3 represents simulation curves for the blood concentration of rifampicin when using different oral doses, together with experimentally obtained values. To confirm the nonlinearity of rifampicin pharmacokinetics, AUC_{0-12h} for 300 mg b.i.d. (twice a day) and 600 mg q.d. (once a day) were calculated (Fig. 4). Even though the total daily dose is the same, the AUC_{0-12h} for 300 mg b.i.d. rifampicin was much smaller than that for 600 mg q.d. This result could be successfully explained by considering it to be a saturable elimination process. Auto-inducible elimination of rifampicin was described by a concentration-dependent increase in V_{max}.

In vitro-in vivo extrapolation

Using Eqs. 15–17, the concentration of unbound rifampicin in the liver was computed. The profile was convoluted into Eq. 6 to estimate CYP3A4 induction under clinical conditions, assuming that the mechanism of CYP3A4 induction is equivalent between *in vitro* and *in vivo* states. Fig. 5 shows a simulation of CYP3A4 induction following repeated oral dosing of rifampicin. The level of CYP3A4 activity was transiently increased, peaking on day 4, and then stabilizing on day 6 or later. Fluctuation of CYP3A4 activity arising from repeated dosing of rifampicin was minimal, unlike that of the blood concentration of the drug. Therefore, a static model for enzyme induction would be sufficient to describe the DDI occurring after rifampicin has been repeatedly administered for more than 5 days.

Table 1 summarizes clinical DDI results between rifampicin and drugs known to be metabolized by CYP3A4. The *IR* values were estimated as an average of CYP3A4 activity induction for the day studied, according to the dose, dosing interval, and number of days treated with rifampicin. Using *IR* and fm_{CYP3A4} for each drug, reduction of *AUC* because of co-administration of rifampicin was calculated and compared with clinical data (Fig. 6). The predictive correlation coefficient (Q^2) and standard deviation of prediction errors (*SDEP*) were 0.684 and 0.0630, respectively. Thus, the reduction of *AUC* for various drugs was predicted with fairly good accuracy when using *in vitro* parameters for CYP3A4 induction.

For comparison, prediction using an indirect effect model was conducted. When the default k_{deg} value of the Simcyp simulator (0.0072 h^{-1}) and its corrected value for an *in vitro-in vivo* correlation (0.03 h^{-1}) were used [51,52], the Q^2 values were 0.499 and 0.570, respectively. In addition, the Q^2 values were estimated to be 0.604 when the prediction was made by a simple static model, where the average concentration of rifampicin in blood was calculated by dividing its *AUC* by the dosing interval (i.e., 24 h). The predictions provided by both cases were not as accurate as the presently proposed model.

Simulation of non-steady state DDI using the PHML model

Taking alprazolam as an example, of which the DDI was investigated under short-term treatment with rifampicin, the early phase of DDI was simulated. PBPK parameters for alprazolam (see Table S2) were obtained by curve-fitting to its blood concentration profile as has been reported previously [7], and PBPK models for alprazolam and rifampicin were implemented in PHML using PhysioDesigner. Fig. 7A shows simulations of the blood concentration of alprazolam in the presence and absence of co-administration of rifampicin. Both drugs were assumed to be

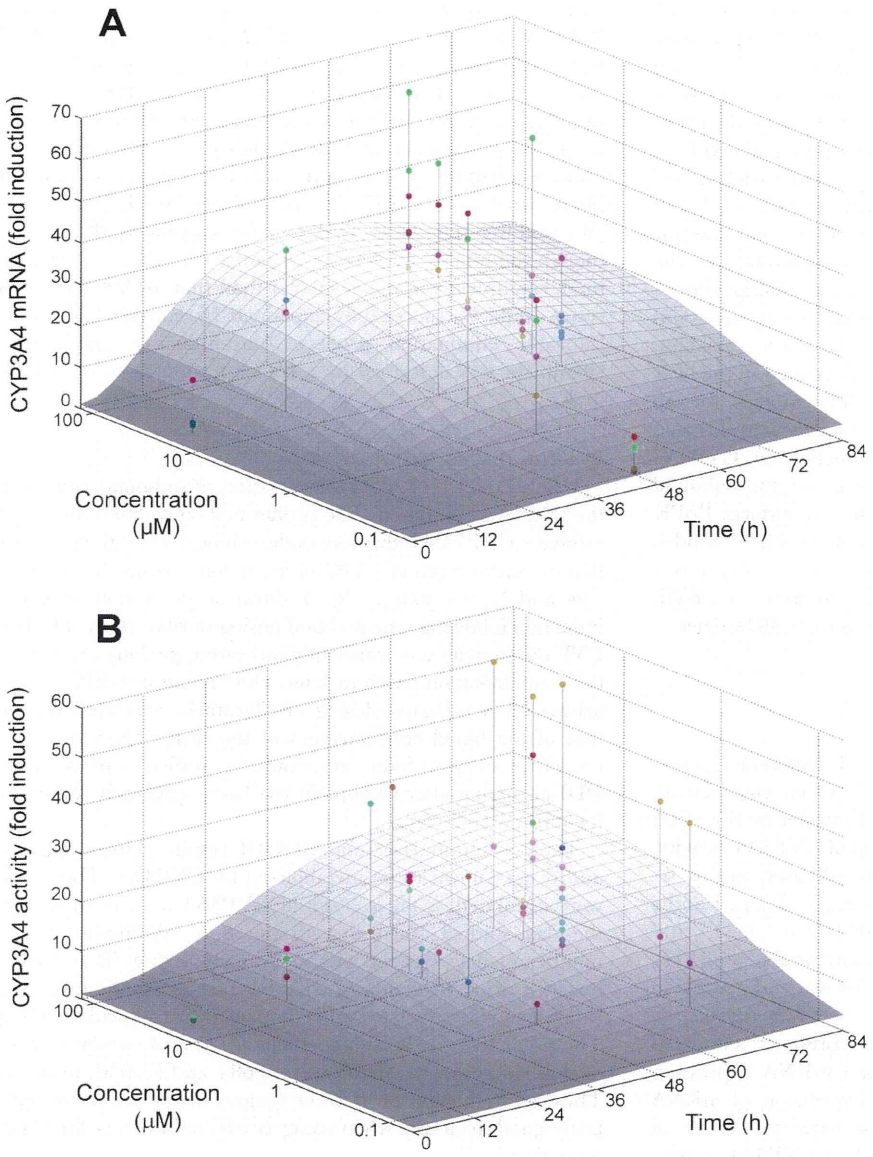

Figure 2. Curve-fitting to experimental data of the induction of CYP3A4 by rifampicin in human hepatocytes. Fig. 2A represents the relative fold induction of CYP3A4 mRNA, while Fig. 2B represents that of the protein level determined by enzyme activity measurements. The data for each donor is presented in a different color. The baseline-normalized data and corresponding equations, i.e., Equations 6–8, were used for this analysis, assuming that inter-individual variability for induction is because of differences in baseline CYP3A4 activity. The surface curves represent the averages.

doi:10.1371/journal.pone.0070330.g002

administered orally every 24 h. In the absence of rifampicin, the blood concentration of alprazolam was increased stepwise following repeated oral doses and eventually reached a steady state. In contrast, in the presence of rifampicin the blood concentration of alprazolam decreased in a time-dependent manner and then reached a steady state at the lower level. Fig. 7B represents comparison between simulation results and measured clinical data [35]. The concentration profile of alprazolam with rifampicin treatment was predicted well (*SDEP*: 0.760), using pharmacokinetic parameters of both drugs and induction dynamics parameters for rifampicin. Pharmacokinetics of other drugs with relatively shorter-term rifampicin treatment were also simulated (see Figure S1), if the time-course data were available.

Discussion

Rifampicin is a strong inducer of drug metabolizing enzymes such as CYP3A4. Rifampicin binds to the nuclear receptor pregnane X receptor (PXR). Once activated, PXR forms a heterodimer with the retinoic receptor (RXR), translocates into the nucleus, and acts as a transcriptional factor. Transactivation of PXR by rifampicin is regulated in a complex manner. Rifampicin-activated PXR is negatively regulated by the small heterodimer partner (SHP), which can be induced by farnesoid X receptor (FXR) ligands [53]. SHP was shown to prevent the PXR/RXR heterodimer from binding to DNA in a pull-down assay, while over-expression of SHP inhibited transactivation of PXR by rifampicin [53]. However, rifampicin-activated PXR is known to suppress expression of the SHP gene, while simultaneously

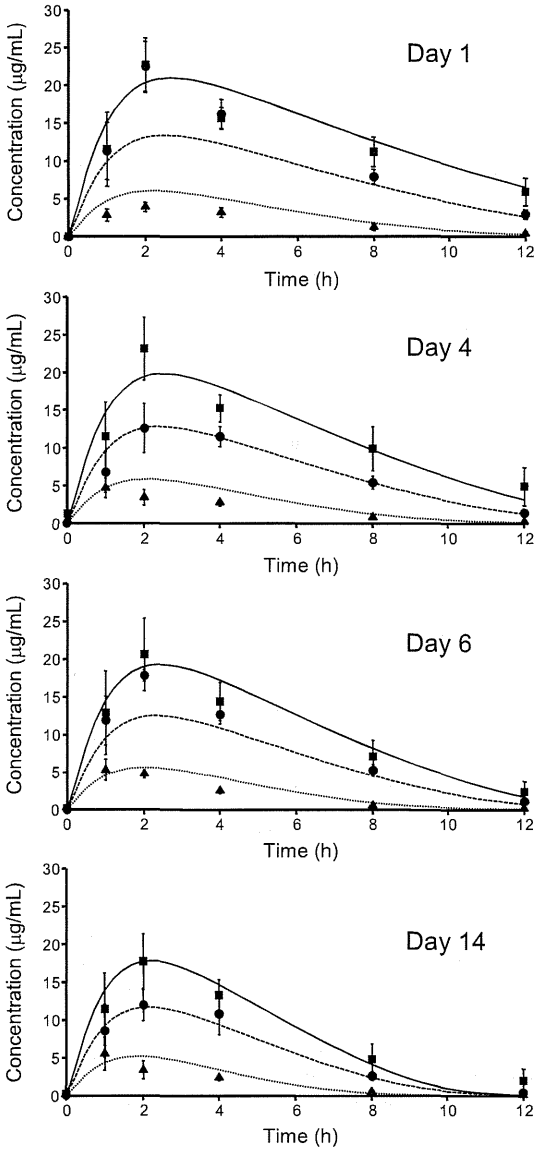

Figure 3. Nonlinear curve-fitting to the blood concentration of rifampicin with repeated oral administration. Clinical data measured on day 1, 4, 6, and 14 (Ref. 40) were simultaneously analyzed based on a PBPK model considering an auto-inducible metabolic process (Eqs. 15–17). Theoretical curves are represented for each data set. Keys: 300 mg, b.i.d. (▲, dotted line); 600 mg, q.d. (●, broken line); 900 mg q.d. (■, solid line).
doi:10.1371/journal.pone.0070330.g003

interacting with HNF4α, SRC-1 and PGC-1α to initiate transcription of the CYP3A4 gene [54]. As shown in Fig. 2, the levels of CYP3A4 mRNA post administration of rifampicin (using data compiled from the literature), appear to be highest at around 48 h. In the present analysis, these observations were regarded as a consequence of gene expression regulatory networks and were described using a simplified negative feedback model.

It has been observed that upon repeated oral administration, the clearance of rifampicin increases because of self-induced metabolism [41,47]. Since the enzyme responsible for the metabolism of rifampicin has recently been identified [55], it is still unclear whether its expression can be induced by a PXR-mediated mechanism, similar to CYP3A4 and other drug metabolizing enzymes [56–58]. Therefore, in order to construct a PBPK model

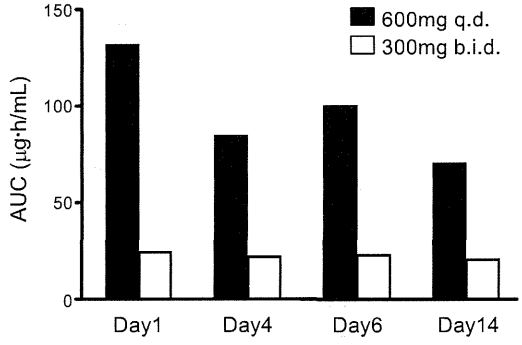

Figure 4. *AUC* measurements of the blood concentration-time profile for oral rifampicin with different dosage regimens. The *AUC* values were calculated from clinical data (Ref. 40) using a trapezoidal method. Note that 600 mg q.d. and 300 mg b.i.d. are the same in terms of total daily dose.
doi:10.1371/journal.pone.0070330.g004

for the analysis of rifampicin pharmacokinetics, a simple auto-induction process was considered. Based on the blood concentration profiles of rifampicin following repeated oral dosing, seven parameters for rifampicin were estimated. Simultaneous multiple curve-fitting allowed robust estimation of the pharmacokinetic parameters. Even the $K_{p,h}$ appeared to be reasonably estimated, despite the lack of hepatic distribution data. The $K_{p,h}$ obtained from the nonlinear regression analysis was 10.6, which fell within the range of $K_{p,h}$ values calculated from *in vivo* human biopsy data (4.8–30.3) [59]. This was also confirmed using the tissue composition-based equations reported by Poulin and Theil [60]. The $K_{p,h}$ for rifampicin was estimated at 6.01 using a computed octanol/water partition coefficient for rifampicin ($\log K_{ow}$: 4.24, obtained from EPI Suite, available at http://www.epa.gov/opptintr/exposure/pubs/episuite.htm).

In vitro parameters for rifampicin were estimated assuming that

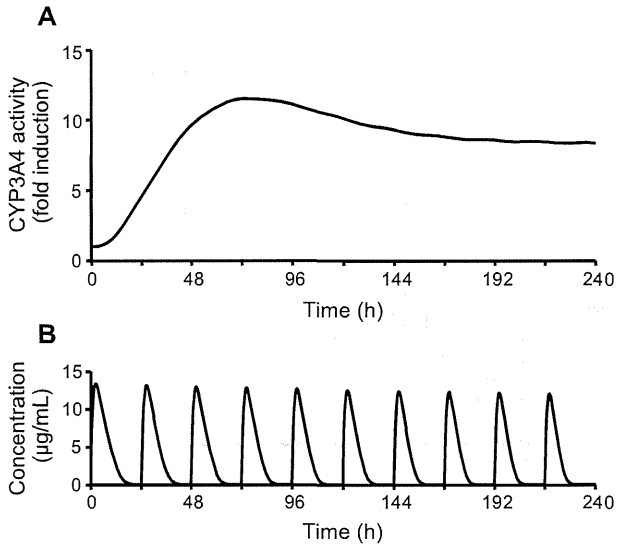

Figure 5. Simulation of the induction of CYP3A4 following repeated oral dosing of rifampicin. Fig. 5A represents the relative fold induction of CYP3A4 enzyme activity, while Fig. 5B represents the blood concentration of rifampicin following oral dosing of 600 mg q.d.. Equations 6–8 and 15–17 were used for this simulation.
doi:10.1371/journal.pone.0070330.g005

Table 1. Prediction of DDIs for various CYP3A4 substrate drugs with concomitantly administered rifampicin.

Substrate		clinical DDI[b]				predicted DDI[c]	
name	fm_{CYP3A4}[a]	daily dose of rifampicin (mg)	days	AUC ratio	Ref. ID	induction ratio (IR) of CYP3A4 activity	AUC ratio
alprazolam	0.75	450	4	0.12	35	9.25 (6.51–19.0)	0.14
atorvastatin	0.68	600	5	0.20	25	9.64 (6.81–19.7)	0.15
buspirone	0.99	600	5	0.088	28	9.64 (6.81–19.7)	0.10
cyclosporine	0.80	600	11	0.27	36	8.16 (5.81–16.5)	0.15
gefitinib	0.39	600	16	0.17	31	7.68 (5.48–15.5)	0.28
imatinib	0.28	600	11	0.26	26	8.16 (5.81–16.5)	0.33
mefloquine	0.44	600	7	0.32	38	8.63 (6.14–17.5)	0.23
midazolam	0.92	600	5	0.041	40	9.64 (6.81–19.7)	0.11
midazolam	0.92	600	9	0.12	27	8.36 (5.94–16.9)	0.13
nifedipine	0.78	600	7	0.082	37	8.63 (6.14–17.5)	0.14
prednisolone	0.18	480	30	0.49	30	6.55 (4.71–13.1)	0.50
simvastatin	1.00	600	9	0.090	27	8.36 (5.94–16.9)	0.12
simvastatin	1.00	600	5	0.14	29	9.64 (6.81–19.7)	0.10
telithromycin	0.49	600	7	0.14	39	8.63 (6.14–17.5)	0.21
triazolam	0.93	600	5	0.051	34	9.64 (6.81–19.7)	0.11
zolpidem	0.40	600	5	0.28	33	9.64 (6.81–19.7)	0.22
zopiclone	0.44	600	5	0.18	32	9.64 (6.81–19.7)	0.21

a) Fraction of the drug metabolized by CYP3A4 (fmCYP3A4) and clinical DDI data were taken from the article of Ohno et al. [24].
b) Clinical data were obtained from the articles shown with the reference ID (Ref. ID).
c) Induction ratio (IR) of CYP3A4 activity was calculated from daily dose and days of administration of rifampicin by using Eqs. 6–8 and 15–17. The values for IR were represented as an average and upper and lower limits when one S.D. for inter-individual variability of CYP3A4 baseline activity was considered.
doi:10.1371/journal.pone.0070330.t001

its degradation was negligible during the time period of the experiment. Even when the metabolism of rifampicin was incorporated into the *in vitro* CYP3A4 induction model using a reported generation rate of the metabolite [58], differences in parameter estimation were at most 16% (data not shown). A notable point of the analysis was that the parameter optimization procedure could be carried out directly without providing the $k_{cyp,deg}$ value. Because it was a parameter sensitive to the difference in the initial slope between the mRNA and activity profiles. In a conventional model which analyzes the activity profile alone, the maximally induced state needs to be presented in the profile to estimate the parameter. More interestingly, the $k_{cyp,deg}$ value estimated (0.0282 h^{-1}) was rather close to 0.03 h^{-1}, which was corrected for better *in vitro/in vivo* extrapolation [51,52], than a default k_{deg} value of the Simcyp simulator (0.0072 h^{-1}). It has been reported that the turnover half-lives for CYP3A4 determined by various methods ranged from 10 to 140 h [61], which corresponds to 0.005–0.07 h^{-1}. Although more information is needed to define an appropriate k_{deg}, the reasonable estimate was obtained from the *in vitro* data.

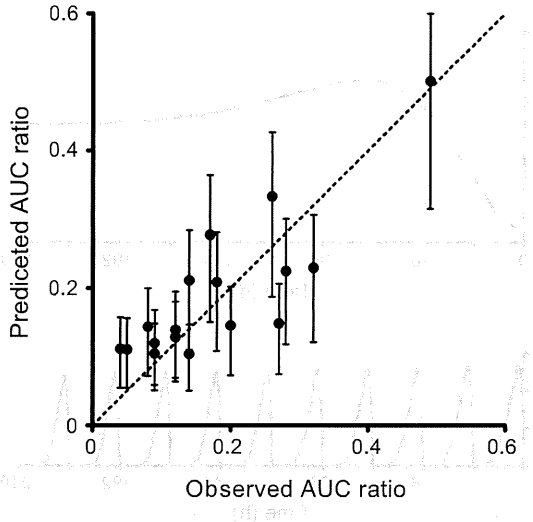

Figure 6. Correlation between predicted and observed *AUC* values for various drugs co-administered with rifampicin. This figure was produced using the values listed in Table 1. Error bars for predicted values represent the standard deviation from the inter-individual variability in baseline CYP3A4 activity. Not that this variability was estimated using extended least squares analysis of *in vitro* data.
doi:10.1371/journal.pone.0070330.g006

The reduction of *AUC* because of rifampicin-induced DDI was satisfactorily predicted from *in vitro* CYP3A4 induction data (Fig. 5). The predictive correlation coefficient of the present dynamic model (Q^2: 0.684) was slightly better than that of a conventionally used indirect effect model with the $k_{cyp,deg}$ of 0.0072 h^{-1} (Q^2: 0.499) or 0.03 h^{-1} (Q^2: 0.570). Since these models can deal with the dynamics of CYP3A4 induction, the IRs for each drug were calculated according to the dosage regimen. As shown in Fig. 5, however, the level of CYP3A4 activity becomes stable on day 6 or later. Since most of the clinical DDI evaluations were carried out on these days (i.e. after 5 or more days of treatment with rifampicin), even a static model could also describe DDI (Q^2: 0.604). The advantage of dynamic models is that it allows the simulation of DDI even at the early stages of treatment. The present dynamic DDI model, which considers the induction of

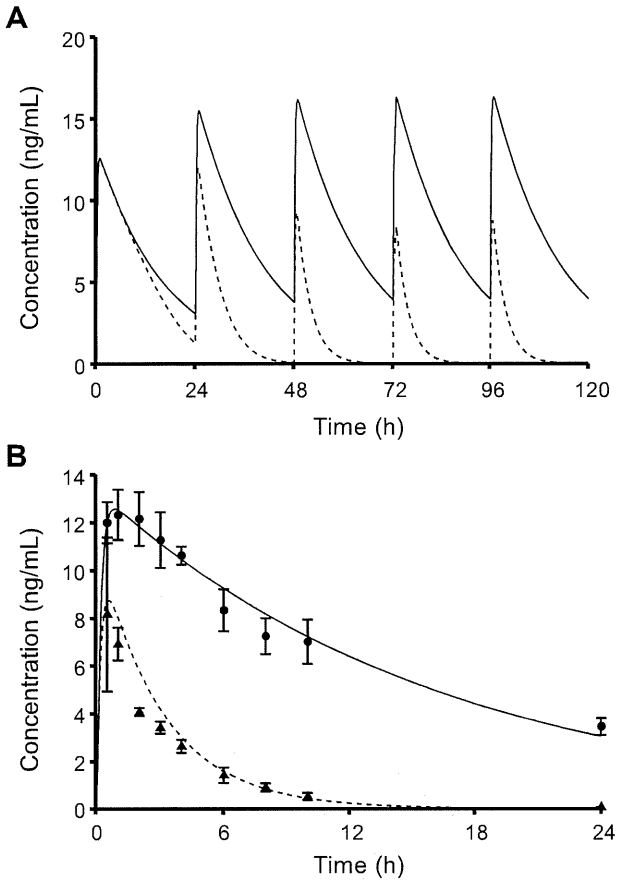

Figure 7. Simulation of DDI between alprazolam and rifampicin using a PHML/SBML hybrid model. Fig. 7A represents blood concentration profiles of repeated oral doses of alprazolam in the absence (solid line) and presence (broken line) of rifampicin. Fig. 7B represents the comparison between the predicted blood concentration of alprazolam with the corresponding clinical data (Ref. 35). Keys: 1 mg alprazolam alone (●, solid line); 1 mg alprazolam with 4-day pretreatment with daily doses of 450 mg rifampicin (▲, broken line). The pharmacokinetic parameters for alprazolam were estimated by curve-fitting to the blood concentrations following the sole administration (standard deviation of residuals, *RSD*: 0.483), and then used for predicting those following the concomitant administration (standard deviation of prediction errors, *SDEP*: 0.760). Both *RSD* and *SDEP* was the same in terms of formula: RSD or $SDEP = \sqrt{\sum (\text{experimental} - calculated)^2} \Big/ n$.
doi:10.1371/journal.pone.0070330.g007

CYP at not only the activity level but also at the mRNA level, was shown to successfully simulate the clearance time-course of alprazolam, a drug known to be metabolized by CYP3A4 (Fig. 7).

Rifampicin is known to induce other CYP enzymes moderately, as has also been described in the FDA guidance [62]. When rifampicin is concomitantly administered, clearance of bupropion (a CYP2B6 substrate), repaglinide (a CYP2C8 substrate), and warfarin (a CYP2C9 substrate) increases 2.1~3.4 times [63], 2.3 times [64], and 2.3~3.8 times [65,66], respectively. As compared with them, clearance of typical CYP3A4 substrates was much more induced (~10 times) (Table 1). A review article [67] compiled information on DDI with rifampicin and indicated that rifampicin induces CYP3A4 more efficiently than other CYPs, glucuronosyltransferases (UGTs), and p-glycoprotein. Taking them into account, induction of other enzymes than CYP3A4 would minimally affect the results of prediction, unless the fm_{CYP3A4} of substrates was extremely low. Gefitinib (fm_{CYP3A4}: 0.39) is known to be metabolized largely by CYP2D6 [68], which is little induced by rifampicin. On the other hand, imatinib (fm_{CYP3A4}: 0.28) is metabolized by CYP2C8 to the similar extent with CYP3A4 [69], resulting in slightly possible underestimation of DDI due to rifampicin. Prednisolone (fm_{CYP3A4}: 0.18) has been reported not to be metabolized by any other CYPs than CYP3A4 or UGTs [70]. Although the reasons why the fm_{CYP3A4} of prednisolone is low remain unclear, the fm_{CYP3A4} of 0.18 gave a good prediction of the DDI due to rifampicin. As long as the results were viewed as fair, induction of other enzymes or transporters might not be important in determining DDI between CYP3A substrates and rifampicin.

PHML, which inherited *insilico*ML (ISML) [71], is a new XML-based specification to describe a wide variety of models of biological and physiological functions with hierarchical structures. It can describe mathematical models consisting of ordinary differential equations, partial differential equations, agent-based simulation models, and others. In a similar way to ISML [71], a model is described by a set of functional elements (modules), each of which specifies mathematical expressions of the module functions. PhysioDesigner acts as a graphical editor and browser of the models written in PHML or ISML. A notable feature of PhysioDesigner is that it provides a function for creating SBML-PHML hybrid models. Since SBML is widely distributed as a standard format for representing and sharing models of biochemical reaction networks, it enables us to create multi-level physiological model systems. The functions of PhysioDesigner allowed us to dynamically connect PBPK-based DDI models with an enzyme transcription/translation dynamics model. Since the module-based hybrid model is highly reusable, extension to more comprehensive network models would be expected in future.

Supporting Information

Figure S1 Simulation of blood concentration of CYP3A4 substrate drugs following their oral administration. Keys: sole administration (●, solid line); 5-day pretreatment with daily doses with 600 mg rifampicin (▲, dash line). Pharmacokinetic parameters for each drug were estimated by curve-fitting to the blood concentrations following the sole administration, and then used for predicting those following co-administration with rifampicin. The pharmacokinetic parameters are given in Table S2.
(DOC)

Table S1 Pharmacokinetic data for CYP3A4 substrates.
(DOC)

Table S2 Pharmacokinetic parameters of CYP3A4 substrates.
(DOC)

Author Contributions

Conceived and designed the experiments: FY HS. Performed the experiments: YS SY AH MH. Analyzed the data: FY. Wrote the paper: FY. Developed the model used in simulation: FY HS. Developed the software used in analysis: YA HK.

References

1. Honig PK, Wortham DC, Zamani K, Conner DP, Mullin JC, et al. (1993) Terfenadine-ketoconazole interaction. Pharmacokinetic and electrocardiographic consequences. JAMA 269: 1513–1518.
2. Josephson F (2010) Drug-drug interactions in the treatment of HIV infection: focus on pharmacokinetic enhancement through CYP3A inhibition. J Intern Med 268: 530–539.
3. Grub S, Bryson H, Goggin T, Lüdin E, Jorga K (2001) The interaction of saquinavir (soft gelatin capsule) with ketoconazole, erythromycin and rifampicin: comparison of the effect in healthy volunteers and in HIV-infected patients. Eur J Clin Pharmacol 57: 115–121.
4. Capone D, Aiello C, Santoro GA, Gentile A, Stanziale P, et al. (1996) Drug interaction between cyclosporine and two antimicrobial agents, josamycin and rifampicin, in organ-transplanted patients. Int J Clin Pharmacol Res 16: 73–76.
5. Lattes R, Radisic M, Rial M, Argento J, Casadei D (1999) Tuberculosis in renal transplant recipients. Transpl Infect Dis 1: 98–104.
6. Modry DL, Stinson EB, Oyer PE, Jamieson SW, Baldwin JC, et al. (1985) Acute rejection and massive cyclosporine requirements in heart transplant recipients treated with rifampin. Transplantation 39: 313–314.
7. Kato M, Shitara Y, Sato H, Yoshisue K, Hirano M, et al. (2008) The quantitative prediction of CYP-mediated drug interaction by physiologically based pharmacokinetic modeling. Pharm Res 25: 1891–1901.
8. Galetin A, Burt H, Gibbons L, Houston JB (2006) Prediction of time-dependent CYP3A4 drug-drug interactions: impact of enzyme degradation, parallel elimination pathways, and intestinal inhibition. Drug Metab Dispos 34: 166–175.
9. Kanamitsu S, Ito K, Sugiyama Y (2000) Quantitative prediction of in vivo drug-drug interactions from in vitro data based on physiological pharmacokinetics: use of maximum unbound concentration of inhibitor at the inlet to the liver. Pharm Res 17: 336–343.
10. Ito K, Brown HS, Houston JB (2004) Database analyses for the prediction of in vivo drug-drug interactions from in vitro data. Br J Clin Pharmacol 57: 473–486.
11. Kato M, Chiba K, Horikawa M, Sugiyama Y (2005) The quantitative prediction of in vivo enzyme-induction caused by drug exposure from in vitro information on human hepatocytes. Drug Metab Pharmacokinet 20: 236–243.
12. Shou M, Hayashi M, Pan Y, Xu Y, Morrissey K, et al. (2008) Modeling, prediction, and in vitro in vivo correlation of CYP3A4 induction. Drug Metab Dispos 36: 2355–2370.
13. Almond LM, Yang J, Jamei M, Tucker GT, Rostami-Hodjegan A (2009) Towards a quantitative framework for the prediction of DDIs arising from cytochrome P450 induction. Curr Drug Metab 10: 420–432.
14. Grime K, Ferguson DD, Riley RJ (2010) The use of HepaRG and human hepatocyte data in predicting CYP induction drug-drug interactions via static equation and dynamic mechanistic modelling approaches. Curr Drug Metab 11: 870–885.
15. Yang J, Liao M, Shou M, Jamei M, Yeo KR, et al. (2008) Cytochrome p450 turnover: regulation of synthesis and degradation, methods for determining rates, and implications for the prediction of drug interactions. Curr Drug Metab 9: 384–394.
16. Fahmi OA, Hurst S, Plowchalk D, Cook J, Guo F, et al. (2009) Comparison of different algorithms for predicting clinical drug-drug interactions, based on the use of CYP3A4 in vitro data: predictions of compounds as precipitants of interaction. Drug Metab Dispos 37: 1658–1666.
17. Zhang JG, Ho T, Callendrello AL, Crespi CL, Stresser DM (2010) A multi-endpoint evaluation of cytochrome P450 1A2, 2B6 and 3A4 induction response in human hepatocyte cultures after treatment with β-naphthoflavone, phenobarbital and rifampicin. Drug Metab Lett 4: 185–194.
18. Pascussi JM, Robert A, Nguyen M, Walrant-Debray O, Garabedian M, et al. (2005) Possible involvement of pregnane X receptor-enhanced CYP24 expression in drug-induced osteomalacia. J Clin Invest 115: 177–186.
19. Parkinson A, Mudra DR, Johnson C, Dwyer A, Carroll KM (2004) The effects of gender, age, ethnicity, and liver cirrhosis on cytochrome P450 enzyme activity in human liver microsomes and inducibility in cultured human hepatocytes. Toxicol Appl Pharmacol 199: 193–209.
20. LeCluyse E, Madan A, Hamilton G, Carroll K, DeHaan R, et al. (2000) Expression and regulation of cytochrome P450 enzymes in primary cultures of human hepatocytes. J Biochem Mol Toxicol 14: 177–188.
21. Sheiner LB, Grasela TH (1984) Experience with NONMEM: analysis of routine phenytoin clinical pharmacokinetic data. Drug Metab Rev 15: 293–303.
22. Sheiner LB, Beal SL (1985) Pharmacokinetic parameter estimates from several least squares procedures: superiority of extended least squares. J Pharmacokinet Biopharm 13: 185–201.
23. Ohno Y, Hisaka A, Suzuki H (2007) General framework for the quantitative prediction of CYP3A4-mediated oral drug interactions based on the AUC increase by coadministration of standard drugs. Clin Pharmacokinet 46: 681–696.
24. Ohno Y, Hisaka A, Ueno M, Suzuki H (2008) General framework for the prediction of oral drug interactions caused by CYP3A4 induction from in vivo information. Clin Pharmacokinet 47: 669–680.
25. Backman JT, Luurila H, Neuvonen M, Neuvonen PJ (2005) Rifampin markedly decreases and gemfibrozil increases the plasma concentrations of atorvastatin and its metabolites. Clin Pharmacol Ther 78: 154–167.
26. Bolton AE, Peng B, Hubert M, Krebs-Brown A, Capdeville R, et al. (2004) Effect of rifampicin on the pharmacokinetics of imatinib mesylate (Gleevec, STI571) in healthy subjects. Cancer Chemother Pharmacol 53: 102–106.
27. Chung E, Nafziger AN, Kazierad DJ, Bertino JS (2006) Comparison of midazolam and simvastatin as cytochrome P450 3A probes. Clin Pharmacol Ther 79: 350–361.
28. Kivistö KT, Lamberg TS, Neuvonen PJ (1999) Interactions of buspirone with itraconazole and rifampicin: effects on the pharmacokinetics of the active 1-(2-pyrimidinyl)-piperazine metabolite of buspirone. Pharmacol Toxicol 84: 94–97.
29. Kyrklund C, Backman JT, Kivistö KT, Neuvonen M, Laitila J, et al. (2000) Rifampin greatly reduces plasma simvastatin and simvastatin acid concentrations. Clin Pharmacol Ther 68: 592–597.
30. McAllister WA, Thompson PJ, Al-Habet SM, Rogers HJ (1983) Rifampicin reduces effectiveness and bioavailability of prednisolone. Br Med J (Clin Res Ed) 286: 923–925.
31. Swaisland HC, Ranson M, Smith RP, Leadbetter J, Laight A, et al. (2005) Pharmacokinetic drug interactions of gefitinib with rifampicin, itraconazole and metoprolol. Clin Pharmacokinet 44: 1067–1081.
32. Villikka K, Kivistö KT, Lamberg TS, Kantola T, Neuvonen PJ (1997) Concentrations and effects of zopiclone are greatly reduced by rifampicin. Br J Clin Pharmacol 43: 471–474.
33. Villikka K, Kivistö KT, Luurila H, Neuvonen PJ (1997) Rifampin reduces plasma concentrations and effects of zolpidem. Clin Pharmacol Ther 62: 629–634.
34. Villikka K, Kivistö KT, Backman JT, Olkkola KT, Neuvonen PJ (1997) Triazolam is ineffective in patients taking rifampin. Clin Pharmacol Ther 61: 8–14.
35. Schmider J, Brockmöller J, Arold G, Bauer S, Roots I (1999) Simultaneous assessment of CYP3A4 and CYP1A2 activity in vivo with alprazolam and caffeine. Pharmacogenetics 9: 725–734.
36. Hebert MF, Roberts JP, Prueksaritanont T, Benet LZ (1992) Bioavailability of cyclosporine with concomitant rifampin administration is markedly less than predicted by hepatic enzyme induction. Clin Pharmacol Ther 52: 453–457.
37. Holtbecker N, Fromm MF, Kroemer HK, Ohnhaus EE, Heidemann H (1996) The nifedipine-rifampin interaction. Evidence for induction of gut wall metabolism. Drug Metab Dispos 24: 1121–1123.
38. Ridtitid W, Wongnawa M, Mahatthanatrakul W, Chaipol P, Sunbhanich M (2000) Effect of rifampin on plasma concentrations of mefloquine in healthy volunteers. J Pharm Pharmacol 52: 1265–1269.
39. Shi J, Montay G, Bhargava VO (2005) Clinical pharmacokinetics of telithromycin, the first ketolide antibacterial. Clin Pharmacokinet 44: 915–934.
40. Backman JT, Olkkola KT, Neuvonen PJ (1996) Rifampin drastically reduces plasma concentrations and effects of oral midazolam. Clin Pharmacol Ther 59: 7–13.
41. Acocella G, Pagani V, Marchetti M, Baroni GC, Nicolis FB (1971) Kinetic studies on rifampicin. I. Serum concentration analysis in subjects treated with different oral doses over a period of two weeks. Chemotherapy 16: 356–370.
42. Garcia M, Rager J, Wang Q, Strab R, Hidalgo IJ, et al. (2003) Cryopreserved human hepatocytes as alternative in vitro model for cytochrome p450 induction studies. In Vitro Cell Dev Biol Anim 39: 283–287.
43. Hariparsad N, Nallani SC, Sane RS, Buckley DJ, Buckley AR, et al. (2004) Induction of CYP3A4 by efavirenz in primary human hepatocytes: comparison with rifampin and phenobarbital. J Clin Pharmacol 44: 1273–1281.
44. Hariparsad N, Carr BA, Evers R, Chu X (2008) Comparison of immortalized Fa2N-4 cells and human hepatocytes as in vitro models for cytochrome P450 induction. Drug Metab Dispos 36: 1046–1055.
45. Li AP, Jurima-Romet M (1997) Applications of primary human hepatocytes in the evaluation of pharmacokinetic drug-drug interactions: evaluation of model drugs terfenadine and rifampin. Cell Biol Toxicol 13: 365–374.
46. Prueksaritanont T, Richards KM, Qiu Y, Strong-Basalyga K, Miller A, et al. (2005) Comparative effects of fibrates on drug metabolizing enzymes in human hepatocytes. Pharm Res 22: 71–78.
47. Acocella G (1978) Clinical pharmacokinetics of rifampicin. Clin Pharmacokinet 3: 108–127.
48. Hucka M, Finney A, Sauro HM, Bolouri H, Doyle JC, et al. (2003) The systems biology markup language (SBML): a medium for representation and exchange of biochemical network models. Bioinformatics 19: 524–531.
49. Ghosh S, Matsuoka Y, Asai Y, Hsin KY, Kitano H (2011) Software for systems biology: from tools to integrated platforms. Nat Rev Genet 12: 821–832.
50. Kitano H, Funahashi A, Matsuoka Y, Oda K (2005) Using process diagrams for the graphical representation of biological networks. Nat Biotechnol 23: 961–966.
51. Wang YH (2010) Confidence assessment of the Simcyp time-based approach and a static mathematical model in predicting clinical drug-drug interactions for mechanism-based CYP3A inhibitors. Drug Metab Dispos 38: 1094–1104.
52. Friedman EJ, Fraser IP, Wang YH, Bergman AJ, Li CC, et al. (2011) Effect of different durations and formulations of diltiazem on the single-dose pharmacokinetics of midazolam: how long do we go? J Clin Pharmacol 51: 1561–1570.
53. Ourlin JC, Lasserre F, Pineau T, Fabre JM, Sa-Cunha A, et al. (2003) The small heterodimer partner interacts with the pregnane X receptor and represses its transcriptional activity. Mol Endocrinol 17: 1693–1703.

54. Li T, Chiang JY (2006) Rifampicin induction of CYP3A4 requires pregnane X receptor cross talk with hepatocyte nuclear factor 4alpha and coactivators, and suppression of small heterodimer partner gene expression. Drug Metab Dispos 34: 756–764.
55. Yang J, Yan B (2007) Photochemotherapeutic agent 8-methoxypsoralen induces cytochrome P450 3A4 and carboxylesterase HCE2: evidence on an involvement of the pregnane X receptor. Toxicol Sci 95: 13–22.
56. Xie W, Yeuh MF, Radominska-Pandya A, Saini SP, Negishi Y, et al. (2003) Control of steroid, heme, and carcinogen metabolism by nuclear pregnane X receptor and constitutive androstane receptor. Proc Natl Acad Sci U S A 100: 4150–4155.
57. Chen Y, Ferguson SS, Negishi M, Goldstein JA (2004) Induction of human CYP2C9 by rifampicin, hyperforin, and phenobarbital is mediated by the pregnane X receptor. J Pharmacol Exp Ther 308: 495–501.
58. Nakajima A, Fukami T, Kobayashi Y, Watanabe A, Nakajima M, et al. (2011) Human arylacetamide deacetylase is responsible for deacetylation of rifamycins: rifampicin, rifabutin, and rifapentine. Biochem Pharmacol 82: 1747–1756.
59. Furesz S, Scotti R, Pallanza R, Mapelli E (1967) Rifampicin: a new rifamycin. 3. Absorption, distribution, and elimination in man. Arzneimittelforschung 17: 534–537.
60. Poulin P, Theil FP (2002) Prediction of pharmacokinetics prior to in vivo studies. 1. Mechanism-based prediction of volume of distribution. J Pharm Sci 91: 129–156.
61. Yang J, Liao M, Shou M, Jamei M, Yeo KR, et al. (2008) Cytochrome P450 turnover: regulation of synthesis and degradation, methods for determining rates, and implications for the prediction of drug interactions. Curr Drug Metab 9: 384–393.
62. Guidance for industry. drug interaction studies – study design, data analysis, implications for dosing, and labeling recommendations. Available: http://www.fda.gov/downloads/Drugs/GuidanceComplianceRegulatoryInformation/Guidances/ucm292362.pdf.
63. Chung JY, Cho JY, Lim HS, Kim JR, Yu KS, et al. (2011) Effects of pregnane X receptor (NR1I2) and CYP2B6 genetic polymorphisms on the induction of bupropion hydroxylation by rifampin. Drug Metab Dispos 39: 92–97.
64. Niemi M, Backman JT, Neuvonen M, Neuvonen PJ, Kivistö KT (2000) Rifampin decreases the plasma concentrations and effects of repaglinide. Clin Pharmacol Ther 68: 495–500.
65. O'Reilly RA (1974) Interaction of sodium warfarin and rifampicin. studies in man. Ann Intern Med 81: 337–340.
66. Heimark LD, Gibaldi M, Trager WF, O'Reilly RA, Goulart DA (1987) The mechanism of the warfarin-rifampin drug interaction in humans. Clin Pharmacol Ther 42:388–394.
67. Chen J, Raymond K (2006) Roles of rifampicin in drug-drug interactions: underlying molecular mechanisms involving the nuclear pregnane X receptor. Ann Clin Microb Antimicrob 5: 3.
68. Li J, Zhao M, He P, Hidalgo M, Baker SD (2007) Differential metabolism of gefitinib and erlotinib by human cytochrome P450 enzymes. Clin Cancer Res 13: 3731–3737.
69. Nebot N, Crettol S, d'Esposito F, Tattam B, Hibbs DE, et al. (2010) Participation of CYP2C8 and CYP3A4 in the N-demethylation of imatinib in human hepatic microsomes. Br J Pharmacol 161: 1059–1069.
70. Zhang ZY, Chen M, Chen J, Padval MV, Kansra VV (2009) Biotransformation and in vitro assessment of metabolism-associated drug–drug interaction for CRx-102, a novel combination drug candidate. J Pharm Biomed Anal 50: 200–209.
71. Asai Y, Suzuki Y, Kido Y, Oka H, Heien E, et al. (2008) Specifications of insilicoML 1.0: a multilevel biophysical model description language. J Physiol Sci 58: 447–458.

Mol Neurobiol (2014) 49:88–102
DOI 10.1007/s12035-013-8489-4

Integrating Pathways of Parkinson's Disease in a Molecular Interaction Map

Kazuhiro A. Fujita · Marek Ostaszewski · Yukiko Matsuoka · Samik Ghosh · Enrico Glaab · Christophe Trefois · Isaac Crespo · Thanneer M. Perumal · Wiktor Jurkowski · Paul M. A. Antony · Nico Diederich · Manuel Buttini · Akihiko Kodama · Venkata P. Satagopam · Serge Eifes · Antonio del Sol · Reinhard Schneider · Hiroaki Kitano · Rudi Balling

Received: 15 April 2013 / Accepted: 13 June 2013 / Published online: 7 July 2013
© The Author(s) 2013. This article is published with open access at Springerlink.com

Abstract Parkinson's disease (PD) is a major neurodegenerative chronic disease, most likely caused by a complex interplay of genetic and environmental factors. Information on various aspects of PD pathogenesis is rapidly increasing and needs to be efficiently organized, so that the resulting data is available for exploration and analysis. Here we introduce a computationally tractable, comprehensive molecular interaction map of PD. This map integrates pathways implicated in PD pathogenesis such as synaptic and mitochondrial dysfunction, impaired protein degradation, alpha-synuclein pathobiology and neuroinflammation. We also present bioinformatics tools for the analysis, enrichment and annotation of the map, allowing the research community to open new avenues in PD research. The PD map is accessible at http://minerva.uni.lu/pd_map.

Keywords Parkinson's disease · Molecular neuropathology · Knowledge repository · Bioinformatics

K. Fujita and M. Ostaszewski contributed equally to this work.

Electronic supplementary material The online version of this article (doi:10.1007/s12035-013-8489-4) contains supplementary material, which is available to authorized users.

Introduction

Parkinson's disease (PD) is a major neurodegenerative disease, characterized clinically by a range of symptoms, in particular, impaired motor behaviour. The pathogenesis of PD is multi-factorial and age-related, implicating various genetic and environmental factors [1]. Gaps in the understanding of the underlying molecular mechanisms hamper the design of effective disease modifying therapies. Investigation of such a complex disease requires a proper knowledge repository that

K. A. Fujita · Y. Matsuoka · S. Ghosh · H. Kitano
The Systems Biology Institute, Minato-ku, Tokyo, Japan

M. Ostaszewski · E. Glaab · C. Trefois · I. Crespo · T. M. Perumal · W. Jurkowski · P. M. A. Antony · N. Diederich · M. Buttini · V. P. Satagopam · S. Eifes · A. del Sol · R. Schneider · R. Balling (✉)
Luxembourg Centre for Systems Biomedicine (LCSB), University of Luxembourg, 7, Avenue des Hauts-Fourneaux, Esch-sur-Alzette, Luxembourg
e-mail: rudi.balling@uni.lu

M. Ostaszewski
Integrated Biobank of Luxembourg, Luxembourg City, Luxembourg

N. Diederich
Department of Neuroscience, Centre Hospitalier Luxembourg, Luxembourg City, Luxembourg

A. Kodama
Faculty of Medicine, Tokyo Medical and Dental University, Tokyo, Japan

V. P. Satagopam · R. Schneider
Computational Biology Unit, European Molecular Biology Laboratory, Heidelberg, Germany

H. Kitano
Sony Computer Science Laboratories, Shinagawa-ku, Tokyo, Japan

H. Kitano
Division of Systems Biology, Cancer Institute, Tokyo, Japan

H. Kitano
Open Biology Unit, Okinawa Institute of Science and Technology, Kunigami, Okinawa, Japan

organizes the rapidly growing PD-related knowledge — a disease map.

The concept of a disease map is relatively new and has found only a limited application in the field of neurodegenerative diseases thus far [2, 3]. Such a map represents diagrammatically interactions between molecular components and pathways reported to play a role in disease pathogenesis and progression. It provides navigation and exploration tools that help the user to locate specific areas of interest and visualize known interactions. Associated analytical tools allow investigators to develop a profound understanding of the disease, detect unexpected interactions and ultimately identify new research hypotheses.

In this paper, we present a PD molecular interaction map that captures and visualizes all major molecular pathways involved in PD pathogenesis. Furthermore, it constitutes a resource for computational analyses and a platform for community level collaborations [4, 5] (see Fig. 1). We also present how a set of bioinformatics tools applied to the map can facilitate in-depth knowledge extraction and continuous curation.

The paper is divided into two parts. In the first part, we review the pathways implicated in PD, with a focus on synaptic and mitochondrial dysfunction, α-synuclein pathobiology, failure of protein degradation systems, neuroinflammation and apoptosis. In the second part of the paper, we demonstrate how the PD map interfaces with bioinformatics tools and databases for its content annotation, enrichment with experimental results, and analysis of its complex structure and dynamics. The PD map is accessible under http://minerva.uni.lu/pd_map (Online resource 1), as a SBML file (Online resource 2), and Payao, a community platform for pathway model curation [264].

Neurodegeneration in Parkinson's Disease Arises from Dysregulation of Interlinked Molecular Pathways

The major pathological feature of PD is the progressive degeneration of the nigrostriatal system, leading to the loss of dopaminergic (DA) neurons in the substantia nigra pars compacta (SNpc) [6]. The degeneration of the nigrostriatal pathway and subsequent loss of striatal dopamine contributes to the cardinal clinical motor symptoms: tremor, rigidity, bradykinesia and postural instability [7]. Although treatments such as dopamine substitution and deep brain stimulation alleviate many of the motor symptoms, there is no disease-modifying therapy preventing the progressive loss of DA neurons [8].

Susceptibility for PD is modulated by various environmental factors [9–13], genetic predisposition or risk factors [14] and epigenetic alterations [15, 16].[1] Exposure to pesticides and industrial agents has been associated with an increased risk for PD [17, 18], but to date none of these agents have been consistently identified as a causal factor for PD [19]. It is known that exposure to inhibitors of mitochondrial respiration [20–25] are sufficient to induce PD symptoms in humans and DA neurodegeneration in animal models.

In this paper, we focus on DA neurons as a major point of convergence in PD disease pathways. However, pathogenic pathways leading to the demise of DA neurons may impact any neuronal population affected in PD, including those of the autonomic ganglia [26, 27]. The demise of these populations may contribute to a range of PD-typical non-motor symptoms hampering the life of PD patients, such as constipation and dysautonomia (ganglia of autonomous nervous system), cognitive decline and REM sleep behaviour (cholinergic neurons of the nucleus basalis of Meynert, noradrenergic coeruleus–subcoeruleus complex), depression and apathy (serotinergic caudal raphe nuclei, cholinergic gigantocellular reticular nucleus) [28, 29].

Vulnerability and Preferential Loss of Midbrain Dopaminergic Neurons

SNpc DA neurons are the most vulnerable population of neurons in PD. It has been suggested that their loss is multifactorial and related to the characteristic features of these cells: complex morphology, high energy demand, high calcium flux, and dopamine metabolism [30]. Consequently, these neurons are particularly susceptible to various stressors, which contribute to their preferential loss (see Fig. 2).

SNpc DA neurons have one of the longest yet most dense arborisation of all neurons [31, 32]. They project to the striatum, providing it with DA [33, 34]. These neurons have long, thin, mostly unmyelineated axons [35] and up to 150,000 presynaptic terminals per neuron [30]. The high energy demand required to support synaptic activity, compensation for the potential risk of depolarization in the unmyelinated membrane, and axonal transport over long distances put a huge burden on the mitochondria. Interestingly, toxins that perturb the energy production and the axonal transport of mitochondria [36], cause parkinsonism in humans and preferential loss of DA neurons in animal models [22, 36, 37]. Finally, the large number of synapses increases the risk for local α-synuclein (α-syn) misfolding (see sections "Synaptic Dysfunction" and "α-Synuclein Misfolding and Pathobiology").

SNpc DA neurons can fire autonomously and have specific calcium L-type Cav 1.3 channels that regulate this pacemaking activity [38, 39]. The resulting high intracytosolic Ca^{2+} concentrations induce cellular stress, elevate the levels of reactive oxygen species (ROS), and increase demand for calcium buffering, which is handled by the endoplasmic reticulum (ER) and the mitochondria. Maintaining proper calcium homeostasis in such an environment increases again the

[1] Epigenetic alterations — secondary, environmentally induced changes of gene expression.

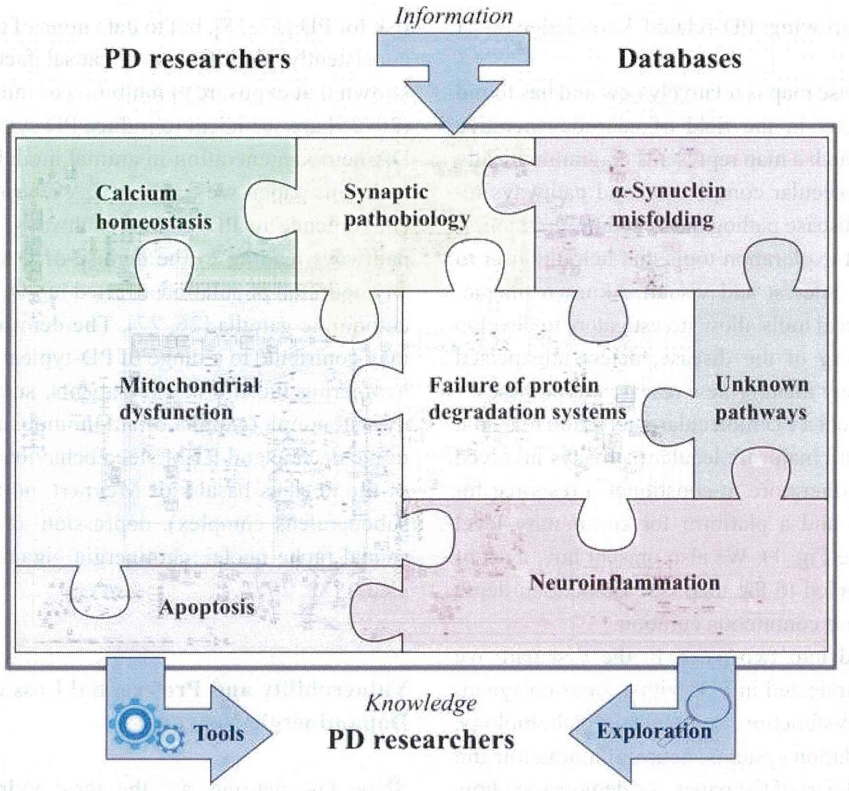

Fig. 1 The concept of Parkinson's disease map and its possibilities. The PD map is a knowledge repository bringing together different molecular mechanisms and pathways considered to be the key players in the disease. The current focus of the map is illustrated by the pieces in the "PD puzzle" These modules include synaptic and mitochondrial dysfunction, failure of protein degradation systems, α-synuclein pathobiology and misfolding, and neuroinflammation. Processes important in PD-associated neurodegeneration, such calcium homeostasis or apoptosis, are discussed within their appropriate context in the main text, and included into the PD map pathways. The PD map is represented as a graph constructed with all gene-regulatory protein and metabolic interactions extracted from published data. Currently the map has 2,285 elements and 989 reactions supported by 429 articles and 254 entries from publicly available bioinformatic databases. It is compliant with standardized graphical representation, Systems Biology Graphical Notation (*SBGN*) [265]. This standardized representation of the map could become a common language for the PD research community to discuss disease-related molecular mechanisms [5]. Detailed contents of the PD map are accessible at http://minerva.uni.lu/MapViewer/map?id=pdmap (Online resource 1) as an SBML file (Online resource 2) and in Payao [264]. The map can be updated with information from the PD research community, as well as by searching bioinformatics databases. Exploration and analysis of the content has the potential to broaden knowledge on the molecular processes in PD, generate of new hypotheses on disease pathogenesis, or prioritize the most interesting areas and molecules for investigation. Approaches to facilitate this knowledge acquisition process are discussed in detail in the section "Annotation, enrichment and Analysis of the PD Map"

energy needs. In contrast, neighbouring dopamine neurons in the ventral tegmental area use Na^+ channels for pacemaking and are relatively spared in PD [37].

Cytosolic DA also contributes to the vulnerability of DA neurons, primarily because its metabolism induces oxidative and nitrative stress in an age-dependent manner [40–42]. Neurotoxicity of DA increases with its concentration, which is thought to be regulated by Ca^{2+} concentration [43]. Additionally, dopamine metabolism is involved in a number of PD-associated pathways, as it can impair synapse function, inhibit protein degradation and disturb mitochondrial dynamics by inhibiting the function of Parkin.

Ageing, the primary risk factor for PD, especially affects DA neurons (see Fig. 2). α-Syn accumulation increases with age in the SNpc and correlates with the loss of DA neurons in non-human primates [42]. This could be linked to the age-related impairment of the two protein degradation systems: the ubiquitin–proteasome system (UPS) [42] and the autophagy–lysosome system [44]. ROS accumulate in an ageing brain [42, 45], partially due to mitochondria dysfunction, as mitophagy[2] is decreased with ageing [45, 46]. Finally, the threshold required to trigger a neuroinflammatory response may decrease with age, since glial activation in SNpc increases in the ageing brain [42, 47].

Synaptic Dysfunction

The main function of a synapse is to establish a connection between neurons allowing communication via chemical or

[2] Mitophagy — autophagy of mitochondria.

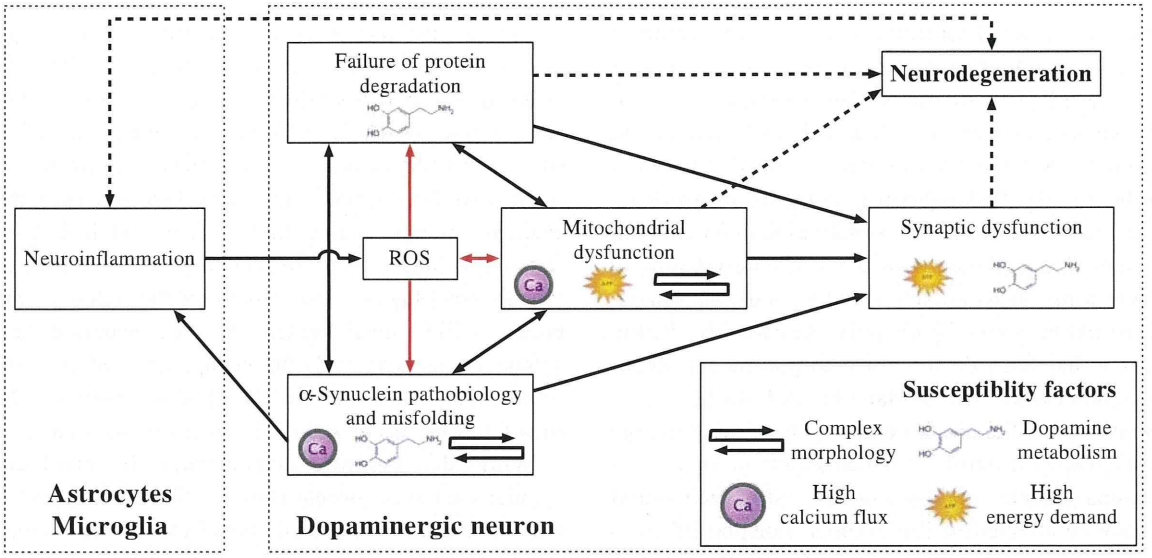

Fig. 2 Pathways implicated in PD and their relationship to susceptibility factors of SNpc DA neurons. The *black arrows* represent direct molecular interactions between the dysregulated pathways. *Red arrows* denote pathways affected by or generating ROS. *Dashed lines* represent indirect associations of these pathways and neurodegeneration. Susceptibility factors of SNpc DA neurons associated with a given pathway are indicated by their corresponding symbols

electric signals. The synapse has emerged as a neuronal structure highly susceptible to a variety of chronic insults [48–51]. Below, we discuss the increasing evidence indicating that synapses are also affected in PD, and that their dysfunction and demise contributes to the disease.

α-Syn is a presynaptic protein. Point mutations, duplications or triplications of its gene are associated with familial PD [52–54]. In cultured neurons, it transiently associates with synaptic vesicles prior to neurotransmitter release, upon which it rapidly redistributes to the cytosol [55]. Association of α-syn with the synaptic vesicle may occur through its binding to SNARE complex proteins [56], and, as shown in mice, α-syn positively influences functional SNARE levels [57]. Similarly, upregulation of α-syn in synapses and cell somas of cultured neurons protects against oxidative stress [58]. However, the protective effect of α-syn is limited to a narrow concentration range, since high levels of α-syn cause familial PD [53]. Even modest overexpression of α-syn has been reported to markedly inhibit neurotransmitter release [59]. Also, α-syn forms potentially pathogenic microaggregates in the synapse [60]. Another protein involved familial and sporadic PD, LRRK2, is also present in the synapse. Its experimentally induced upregulation or knockdown impairs the dynamics of synaptic vesicle release and recycling [61, 62]. However, the influence of mutated or dysfunctional LRRK2 on these processes in PD remains to be investigated.

A number of other PD-related pathological events might affect synapses. Synapses of the nigrostriatal pathway, with their high level of α-syn and dopamine, are likely to be the major site of the formation of toxic adducts of α-syn and oxidized DA [40, 63, 64]. Furthermore, the energy demands of synapses may be compromised by dysfunctional mitochondrial respiration, turnover, or axonal transport [65]. Locally dysfunctional protein degradation and turnover may directly affect synaptic function and plasticity [66].

Mitochondrial Dysfunction

Mitochondria are highly dynamic organelles essential for a range of cellular processes including ATP production, ROS management, calcium homeostasis, and control of apoptosis. The maintenance of mitochondrial homoeostasis by mitophagy involves multiple factors ranging from the control of mitochondrial fusion and fission to mitochondrial motility [67]. These processes are strongly related to proteins involved in familial and sporadic PD [65, 68, 69].

A number of proteins associated with familial PD are related to mitochondrial function [70], with PINK1 and Parkin playing a particularly important role. Control of mitochondrial turnover and protection against oxidative stress are mediated via the kinase activity of PINK1 targeting Parkin [71], HTRA2 [72] and TRAP1[73] proteins. In turn, mitophagy is driven by PINK1-mediated translocation of Parkin from the cytosol to mitochondria [71, 74]. Importantly, both mitophagy [75, 76] and transcriptional control of mitochondrial biogenesis [77–79] depend on the E3 ubiquitin ligase activity of Parkin.

Familial PD genes are also implicated in ROS production by mitochondria. Mitochondrial respiration and calcium balance are perturbed by PINK1 deficiency [80, 81]. The resulting reduced mitochondrial calcium capacity and increased ROS